Journal of Molecular Liquids 427 (2025) 127442

Contents lists available at ScienceDirect

Journal of Molecular Liquids

journal homepage: www.elsevier.com/locate/molliq

Unveiling the behavior of cubic and reverse hexagonal liquid crystalline nanoparticles in cellular and skin delivery of glucocorticoid and small interfering RNA

Ana Vitória Pupo Silvestrini [a], Ualisson José da Silva [a], Márcia Carvalho de Abreu Fantini [b], Maria Vitória Lopes Badra Bentley [a,*]

[a] School of Pharmaceutical Sciences of Ribeirão Preto, University of São Paulo, 14040-903 Ribeirão Preto, SP, Brazil
[b] Institute of Physics, University of Sao Paulo, 05508-900 São Paulo, SP, Brazil

ARTICLE INFO

Keywords:
Skin delivery
Liquid crystalline nanoparticle
Co-delivery
Dexamethasone
RNA interference
Small interfering RNA

ABSTRACT

Inflammatory skin diseases affect a large part of the population, often requiring topical anti-inflammatory and immunomodulatory medications. However, managing chronic inflammation typically necessitates high and frequent doses, leading to undesirable short- and long-term side effects. Given the advantages of drug co-administration in nanostructured systems, we developed hexagonal and cubic bicontinuous liquid crystalline nanoparticles (HexLCN/CubLCN) co-loaded with dexamethasone acetate (DMA) and small interfering RNA targeting TNFα (siTNFα) and explored their properties for topical and cellular delivery. The physicochemical characterization confirmed the internal liquid-crystalline mesostructure of the LCNs (Pn3m and H_{II}) and revealed particles sizes between 144 and 166 nm, low polydispersity (0.11–0.18) and positive zeta potential (12.6–16.8 mV). Both LCNs achieved over 95 % DMA encapsulation efficiency and demonstrated strong siRNA binding capacity. Using dermatomized porcine skin, HexLCN showed superior performance, promoting >15-fold greater DMA penetration in the epidermis compared to CubLCN. Similarly, HexLCN facilitated enhanced siRNA delivery, as visualized through confocal laser scanning microscopy (CLSM). In Raw264.7 monocyte/macrophage cells, HexLCN-siRNA complexes achieved a 2- to 3-fold increase in siRNA internalization compared to CubLCN. Finally, therapeutic efficacy was validated in macrophages stimulated with lipopolysaccharide (LPS), where HexLCN-DMA-siTNFα significantly reduced TNFα secretion across all conditions (stimulation and concomitant treatment, pre-stimulation with LPS or stimulation after treatment). The combination of DMA and siTNFα maintained TNFα levels similar to the basal control, which represents a decrease of approximately 6-fold compared to the LPS-control. These findings demonstrate that HexLCNs are promising platforms for the co-delivery of nucleic acids and glucocorticoids, offering potential as therapies for complex inflammatory skin diseases.

1. Introduction

Although the chemical and physiological changes associated with inflammation are an integral process necessary for homeostasis and survival, a dysregulated immune system is implicated in a wide range of diseases [1]. Inflammatory skin diseases such as psoriasis, dermatitis and others affect a large part of the population and represent a high human and economic burden; therapeutic resources for effective therapy are limited [2–4]. Topical treatment is preferable in many cases due to the accessibility and safety. Although the stratum corneum (SC), the main skin barrier, is breached in these diseases, delivering adequate doses of drugs to the diseased skin site is a major challenge due to the complex and highly selective structure of the skin. To overcome the SC and reach the other skin layers, different approaches have been reported in the literature, with emphasis on drug delivery systems based on nanoparticles [5–7]. Lipid nanoparticles are widely used for topical drug delivery due to their biocompatibility, biodegradability, controlled drug release, and ease of scalable production. Recent advances in the design of drug and nucleic acid delivery systems have contributed to the development of non-lamellar liquid crystalline nanoparticles (LCNs),

* Corresponding author at: Av. do Cafe, s/n, 14040-903 Ribeirão Preto, SP, Brazil.
E-mail address: vbentley@usp.br (M.V.L.B. Bentley).

https://doi.org/10.1016/j.molliq.2025.127442
Received 22 August 2024; Received in revised form 16 March 2025; Accepted 21 March 2025
Available online 23 March 2025

also known as cubosomes and hexosomes [8,9].

This prospective class of nanoparticles for drug delivery is formed from lyotropic liquid crystalline (LLC) mesophases, which comprise a thermodynamic intermediate state between the isotropic liquid state and the crystalline solid state [10]. These highly ordered structures are formed as a function of the complex interplay between the molecular shape of the amphiphiles, the total free energy of the lipid-water system, and the environmental conditions. Among the various types of mesophases, the non-lamellar, such as bicontinuous cubic and reverse hexagonal, present a geometrically ordered internal nanoarchitecture and are of great scientific and technological interest for applications such as drug delivery systems [9,11,12]. Structurally, the bicontinuous cubic mesophases present two non-interconnected water channels separated by three-dimensional lipid bilayers arranged on an infinite periodic minimum surface of the primitive, gyroid, or double diamond type, with the crystallographic space groups *Im3m*, *Ia3d*, and *Pn3m*, respectively [13]. On the other hand, the reverse hexagonal mesophase exhibits two-dimensional anisotropic symmetry and structurally consists of seven individually and densely packed, closed, water-filled cylinders surrounded by a lipid bilayer [8,10]. Due to numerous beneficial properties for topical application, biocompatibility, and the ability to accommodate small and macromolecules, LCNs have been investigated by our research group for the past decades [14–17].

Considering the ability of LCNs to co-deliver drugs and with the aim of achieving pharmacodynamically additive or synergistic effects, we explored the properties of bicontinuous cubic mesophase and reverse hexagonal LCNs (named CubLCN and HexLCN) used as platforms for the delivery of dexamethasone acetate (DMA) and small interfering RNA (siRNA) targeting tumor necrosis factor-alpha (TNFα) as a double-target therapeutic strategy for cutaneous inflammation. DMA is a potent synthetic lipophilic glucocorticoid often used in the treatment of inflammatory and allergic skin diseases. It exerts its anti-inflammatory and anti-proliferative effects by targeting the cytoplasmic glucocorticoid receptor (GR). Binding to the GR results in regulation of genomic and non-genomic pathways, leading to changes in gene transcription, protein-receptor interactions, mitochondrial translocation, plasma membrane interactions, and signaling pathways [18,19]. Despite its satisfactory therapeutic effects, the use of DMA is limited to short-term treatment and low doses due to its notorious side effects. In addition, its physicochemical characteristics such as high lipophilicity and molecular size limit its cutaneous penetration, reducing its effectiveness in controlling cutaneous inflammation [20,21]. Therefore, an effective strategy must be developed that allows greater skin penetration and reduces side effects. In this sense, the use of LCNs is particularly attractive as they can improve penetration and bioavailability.

In parallel, siRNA molecules targeting specific targets of the inflammatory cascade (e.g. cytokines and transcription factors) have been considered ideal candidates to treat a range of diseases, including skin diseases [22–25]. Among several cytokines, TNFα plays an important role in the inflammatory cascade. Overproduction of TNFα by macrophages, dendritic cells, and epidermal cells disrupts homeostasis and results in chronic inflammation and cell apoptosis [26,27]. Thus, we hypothesize that post-transcriptional silencing via siRNA to down-regulate TNFα combined with DMA may benefit anti-inflammatory therapy. In RNA interference therapy, exogenous siRNAs in the cytoplasm are incorporated into a multiprotein complex, the RNA induced silencing complex (RISC), which is then oriented through the antisense strand to bind to the homologous sequence of mRNA through Watson-Crick base pairing and completely cleave the target mRNA sequence [25,28,29]. siRNAs are highly selective and effective in silencing the target protein. However, siRNA is a polyvalent and highly hydrophilic anionic molecule of medium size (~13 kDa) with poor pharmacokinetics due to its high susceptibility to enzymatic degradation by endonuclease and low cytoplasmic bioavailability. To overcome these extra- and intra-cellular barriers and deliver therapeutically sufficient amounts to the site of action, the platforms must provide protection against enzymatic degradation [25,30].

Based on these considerations, we sought to explore the influence of the reverse hexagonal and bicontinuous cubic liquid crystalline mesophases on the colloidal properties of their respective LCNs and their abilities to overcome the skin barrier and efficiently deliver DMA and siRNA, as well as allowing increased internalization into target cells. To address this challenge, LCNs with a monoolein-based composition were designed to accommodate DMA in the liquid-crystalline matrix, and their surface was modified with a cationic polymer (poly(allylamine) hydrochloride (PAH)) capable of binding to a siTNFα through electrostatic interactions. The physical–chemical characterization of CubLCN and HexLCN as well as their cellular interactions and TNFα inhibition capacity were described in this manuscript and offer interesting perspectives for this biopharmaceutical innovation.

2. Materials and methods

2.1. Materials

Monoolein (MO; Myverol® 18–99 k) was kindly supplied by Kerry Group (Ireland). DMA was purchased from Fagron (Brazil). Antibiotic and antimycotic solutions (penicillin, streptomycin and amphotericin B), DAPI dye (4′,6-diamidine-2′-phenylindole dihydrochloride), Dulbecco's Modified Eagle Medium (DMEM) culture medium, fetal bovine serum (FBS), oleic acid (OA), PAH (17.5 kDa molecular weight), poloxamer 407 (P407), trypsin-EDTA, resazurin and lipopolysaccharide (LPS) from *Salmonella enterica* sorotype *typhimurium* were obtained from Sigma-Aldrich (USA). Sodium heparin (5000 IU/mL) was obtained from Blausiegel (Brazil). The GelRed® dye (nucleic acid gel stain) was obtained from Biotium, Inc. (USA). RNAse-free water with diethylpyrocarbonate (DEPC), *Silencer*® negative control siRNA (#AM4635) and *Silencer*® pre-engineered siTNFα (sense sequence CGUCGUAGCAAACCACCAATT and antisense sequence UUGGUGGUUUGCUACGACGTG) were obtained from Ambion™ (USA). The siRNA AlexaFluor 647-labeled AllStars Negative Control (siAF647) was obtained from Qiagen® (GER). Mouse ELISA kit was obtained from Invitrogen™ (Thermo Fisher Scientific Inc.). All aqueous solutions were prepared using ultrapure water (pH = 7.4) with a resistivity of 18.2 MΩ·cm from Milli-Q® System by Millipore (Billerica, MA, USA). All analytical reagents were directly used without further purification.

2.2. UV–vis High-performance liquid chromatography (HPLC) method for DMA quantification

A Shimadzu LC-10AD HPLC system coupled with a UV–Vis detector was used for detection and quantification of DMA. The solvent system consisted of a methanol–water mixture (30:70, v/v). Isocratic elution was performed using a reversed-phase C18 column (LiChrospher® 250 RP-18, 250 × 4.6 mm long, 5 μm, LiChrospher; Merck, Germany) and maintained at a temperature of 25 °C and flow rate of 1 mL/min. Chromatograms were obtained at 218 nm, and the sample volume was 20 μL. The method was linear in the concentration range from 0.1 to 20 μg/mL, and the calibration curve was y = 36928x (R^2 = 0.9997). The error and accuracy of the method had a coefficient of variation that did not exceed 10 % and 96–104 %, respectively. The lower limit of quantification of the method was 0.1 μg/mL. The recovery rate of DMA on the skin was greater than 90 %.

2.3. LCN preparation

LCNs were prepared as previously reported [16]. CubLCNs were prepared from the LLC gel formed by MO melted with the aqueous phase (0.01 M sodium phosphate buffer, pH 7.0, containing 1 % P407) at a 8:90 rate (w/w), while the HexLCNs were prepared from the LLC gel formed by MO, OA, and aqueous phase in the ratio 8:1:90 (w/w/w). For cationic LCN, the PAH polymer (0.5 %, w/v) was previously solubilized

in the aqueous phase. DMA was incorporated into the oil phase (0.1 %, w/v) to produce CubLCN-DMA and HexLCN-DMA. After 24 h of equilibration, the gel bulk was sonicated in an ice bath at 30 % maximum power for 1 min (Vibra-Cell™ VCX750, Sonics & Materials, Inc.). For formation of the siRNA-CubLCN/HexLCN complex (N:P ratio of 2:1), exact amounts of the dispersion were mixed with the siRNA solution and left to stand for 30 min before use.

2.4. Polarized light microscopy

Representative aliquots of the liquid crystalline gel after 24 h at equilibrium were analyzed by circular polarized light microscopy using an Axioplan 2 Image Pol microscope (Carl Zeiss, Oberkochen, Germany) equipped with a set of LD-AchroPlan 32x/0.40 objectives, and an Axiocan HRc video camera (Carl Zeiss AG, Germany). All analyses were performed at room temperature.

2.5. Physical-chemical characterization of the LCNs

2.5.1. Hydrodynamic diameter, zeta potential, and nanoparticle concentration

The intensity-weighted average hydrodynamic diameter (Z-average) and polydispersity index (PdI) were analyzed by dynamic light scattering (DLS) using a Malvern Zetasizer Nano (Malvern Instruments, Worcestershire, UK). Correlation graphs generated by the software and the correlogram intercept values (>0.9) were used to measure the reliability of the obtained Gaussian distributions. Measurements of the electrophoretic mobility of the nanoparticles were expressed as zeta potential. All measurements were performed in triplicate at 25 °C using a 1:400 (v/v) dilution in ultrapure water. The means of three determinations in different batches of the same dispersion type were used in the analysis. Measurements of hydrodynamic diameter, PdI, and zeta potential were also performed over a period of 90 days at room temperature (25 °C). The averages of three determinations in three batches of the same dispersion type were used in the analysis.

The LCN concentration (particle number per mL) were determined using a NanoSight NS300 device equipped with a 405 nm laser and a microscope (Malvern Instruments, Worcestershire, UK). For analysis, the samples were diluted in ultrapure water at a ratio of 1:5000 (v/v) and measurements were performed at 25 °C. The results were expressed as particle concentration (average ± standard error) values obtained with NTA software (NTA 3.4 Build 3.4.003).

2.5.2. DMA entrapment efficiency (EE)

The percentage EE of DMA in CubLCN or HexLCN was determined by an ultracentrifugation method. LCN dispersions (1 mL) were centrifuged at 5000 × g for 5 min using Amicon® Ultra-4 (molecular weight cutoff: 50,000 g/mol; EMD Millipore, Darmstadt, Germany), and the filtrate containing free DMA was analyzed using the HPLC system described previously. The EE was calculated according to the formula: EE (%) = [(theoretical concentration − calculated concentration)/theoretical concentration)] × 100.

The content of encapsulated DMA in CubLCN-DMA and HexLCN-DMA was also determined over a period of 90 days at room temperature (25 °C). The averages of three determinations on three batches of the same dispersion type were used in the analysis.

2.5.3. siRNA binding and integrity of the LCN-siRNA complex

The efficiency of siRNA complexing by the CubLCN or HexLCN was assessed by the agarose gel retardation assay. LCN-siRNA complexes were mixed with acid staining and loaded into 2 % agarose gel. To assess siRNA release and its integrity, a heparin solution (5000 IU/mL) was added to the LCN-siRNA complexes for 60 min at 37 °C followed by the addition of nucleic acid staining. For both assays, electrophoresis (Electrophoresis Power Supply, UK) was conducted in 1 × Tris-acetate-EDTA buffer at 120 V for 20 min and images were acquired in a UV light system (Transluminator, Loccus Biotechnology, Brazil) by Quantity One software.

2.5.4. Small angle x-ray scattering (SAXS) analysis

SAXS experiments were performed using Xeuss® 2.0 (Xenocs) system set-up with a Dectris Pilatus 300 k bidimensional detector, operating at a wavelength of 1.5418 Å (copper tube). The sample-detector distance was 0.9 m, and the accessible q range was from 0.015 $Å^{-1}$ to 0.43 $Å^{-1}$. Special glass capillaries (2.0 mm diameter) containing the samples were placed in a temperature-controlled (23 ± 1 °C) sample holder. Prior to each measurement series, a silver behenate standard was used to correct for deviations in the sample-to-detector distance and 0.01 M sodium phosphate buffer (pH 7.0) was used as a background to obtain the absolute scattering intensity. The measured SAXS profiles are displayed as the average intensity I(q) vs. the q-range.

2.6. Release kinetics of DMA-loaded LCN using vertical Franz diffusion cell

The kinetics of DMA release in the formulations was determined using cellulose membrane dialysis (molecular weight cutoff 12000; Himedia Labs, India) in an automatic vertical Franz diffusion cell system (Phoenix®, Teledyne Hanson Research, USA), with a diffusion area of 1.77 cm^2. The receptor solution was composed of 14 mL of 0.01 M sodium phosphate buffer (pH 7.4 ± 0.2) with 10 % ethanol, maintained at 32 °C and 400 rpm constant stirring. An exact volume of 500 μL of the formulations (solution, CubLCN-DMA, and HexLCN-DMA) were applied in the donor compartment and collected at each predetermined time. Samples from the receptor compartment were collected and the amount of DMA was determined by HPLC (n = 6). This assay was performed under infinite dose, occlusion, and sink conditions for 72 h. The cumulative release ($\mu g/cm^2$) versus time (t) was plotted and fitted using the zero-order, first order and Higuchi models.

2.7. In vitro cutaneous permeation and retention of DMA and siRNA co-loaded LCN

In vitro permeation studies were performed using porcine ear skin as the biological membrane (dermatomized at a thickness of 500 μm) according to the OECD Guideline 428 [31]. The samples and conditions were the same as for release kinetics. To assess skin retention in the SC and the epidermis plus dermis (EPD), the skins were removed from the vertical Franz diffusion cell after 24 h of application of the formulations and the surfaces were taped with 15 adhesive tapes, followed by extraction in methanol. The remaining skin (EPD) in methanol were homogenized (Marconi, Turrax MA102, Brazil) and treated in an ultrasonic bath (QUIMIS®, Q3350, Brazil) for 1 min and 20 min, respectively. The extracted DMA was quantified by the HPLC method.

The intensity and penetration depth of the CubLCN or HexLCN complexed with siRNA AF647 (5 μM) into the skin were examined using confocal laser scanning microscopy (CLSM) analysis using Leica TCS SP8 CLSM microscope (Leica Microsystems Inc., Buffalo Grove, USA). Areas exposed to formulations were frozen in Tissue-Tek® (Pelco International, Redding, CA, USA) at −20 °C and cut into 20-μm cross sections in a cryostatic microtome (Leica, Wetzlar, Germany). The histological sections were then stained with DAPI (0.3 μg/mL) for 10 min, and the slides were stored at 4 °C for 12 h. Images were then acquired with an immersion objective of 63 × and lasers of λ = 405 nm and λ = 638 nm suitable for DAPI and AF647, respectively.

2.8. Cell culture

The murine monocyte/macrophage cell line Raw264.7 (ATCC TIB-71) and human immortalized non-tumorigenic keratinocyte cell line HaCaT were grown in Dulbecco's modified Eagle's medium (DMEM) containing 10 % FBS and 1 % antibiotic–antimycotic solution in a

humidified atmosphere of 5 % CO_2 and 95 % air at 37 °C.

2.8.1. Cellular viability assay

Raw264.7 and HaCaT cells were seeded in transparent 96-well plates at 10^4 cells/well and incubated overnight (37 °C, 5 % CO_2). Different concentrations of CubLCN, CubLCN-DMA, HexLCN, and HexLCN-DMA were added to the cells and incubated for 24 h at 37 °C in 5 % CO_2. The medium was subsequently replaced with resazurin reagent solution (25 μg/mL) in cell culture medium. Following 4 h of incubation, the fluorescence was measured in a BioStack Ready (BioTek Synergy 2, USA) according to the manufacturer's conditions (excitation: 530/25, emission: 590/35). The data are expressed as a percentage of viable cells compared to the untreated cells.

2.8.2. Cellular internalization of siRNA-loaded LCN

Fluorescence-activated cell sorting (FACS) and confocal laser scanning microscopy (CLSM) were used to study the cellular internalization of CubLCN-siRNA AF647 and HexLCN-siRNA AF647 and their intracellular distribution in Raw264.7 cells. Briefly, cells were seeded onto a 12-well plate (5×10^5 cells/well) overnight and then incubated for 12 and 24 h with samples at a final concentration of 40 nM siRNA AF647. Cells were also evaluated previously induced with LPS (5 μg/mL) for 1 h before adding the samples. The cell pellet resuspended in PBS was subjected to flow cytometry (BD FACSCanto™ Flow Cytometry System, BD Biosciences, US).

For CLSM analysis, cells were seeded onto 35 mm glass coverslips (10^5 cells/well) overnight. Afterwards, the adhered cells were incubated with the formulations (siRNA AF647 solution, CubLCN-siRNA AF647, and HexLCN-siRNA AF647) and maintained for 24 h at 37 °C in 5 % CO_2. Then, the cells were washed with PBS and fixed with paraformaldehyde (2 %, w/v) for 10 min. The cells were stained with DAPI (0.3 μg/mL) for nuclear staining. Finally, images were acquired using a Leica TCS SP8 CLSM microscope (Leica Microsystems Inc., Buffalo Grove, USA) with a 63 × oil immersion objective and appropriate lasers (excitation/emission: 652/670 nm for AF647 and 358/461 nm for DAPI).

2.8.3. In vitro TNFα downregulation efficiency assay

The anti-inflammatory efficiency of DMA and siTNFα co-loaded HexLCN and respective controls were evaluated based on the amount of secreted TNFα levels after activating the Raw264.7 cells by LPS (500 ng/mL). Cells were seeded onto a 96-well plate (2.5×10^4 cells/well) using full medium and incubated for 24 h at 37 °C. After confirmation of adherence, the cells were submitted to three protocols of LPS-activation and treatment: (1) cells were pre-activated with LPS for 3 h followed by treatments with the formulations for 21 h; (2) cells were incubated simultaneously with LPS and the formulations for 24 h; and (3) cells were incubated with the formulations for 21 h followed by LPS for 3 h. Formulations were used at the following concentrations: DMA solution 1 μM, naked siTNFα 150 nM; HexLCN or HexLCN-DMA (10^8 particles/mL, equivalent to 1 μM DMA) with or without siTNFα 150 nM. At the end of the experiment, supernatants were collected and stored at − 20 °C until the TNFα ELISA, according to the manufacturer's recommended instructions. All measurements were performed in quadruplicate.

2.9. Statistical analysis

All the data are expressed as mean ± standard deviation (SD). Statistical analyses were performed with Graphpad Prism® 9.3.0 software (GraphPad Software, Inc). Detailed sample size and statistical methods used for data analysis of individual studies can be found in the corresponding figure legends. Differences were considered significant at $p < 0.05$.

3. Results and discussion

3.1. LCNs preparation and characterization

In this study, we prepared MO-based LCNs by a top-down approach via ultrasonication, as a well-established methodology in our previous works [14–17]. MO is an unsaturated monoacylglycerol recognized as safe and biocompatible [12,32,33]. At room temperature and an excess of aqueous phase, the amphiphilic MO presents high mesomorphism [33], so it is interesting to produce particles with different internal mesophase structures through subtle changes in the composition, which in turn can impact the external surface structure, colloidal properties, and interactions with biomembranes. Due to its infinite expandability, the LLC bulk can be dispersed in excess aqueous phase in the presence of a stabilizer, usually a non-ionic steric, forming thermodynamically stable nanoparticles [8]. The geometrically ordered internal nanoarchitecture of LCNs is an ideal environment for versatile loading, drug solubilisation, and controlled release functionality [9,12]. Furthermore, its surface can be easily modified for specific targeting and delivery of nucleic acids, as we have shown in our previous studies [12,16].

Considering that the presence of additives can influence the LLC self-organization and the colloidal properties of LCNs, these characteristics were investigated first. In Fig. 1**a**, we show that the precursor LLC bulk formed by MO in excess of aqueous phase with or without PAH polymer and DMA presented an isotropic pattern under polarized light microscopy (Fig. 1**a, 1 to 3**), while the presence of OA together with MO promoted the formation of an anisotropic pattern with characteristic hexagonal mesophase textures. The presence of the cationic polymer and the drug did not alter the birefringence pattern (Fig. 1**a, 4 to 6**). All LCN displayed a white opaque appearance due to strong Rayleigh scattering to visible light and their well-defined structure. The detailed summary of the physicochemical properties of these LCNs is shown in Table 1. NTA measurements of the formed dispersions had an average of 6.1–7.5 × 10^{12} particles/mL for CubLCN and HexLCN, which are in line with previously reported values for LCN generated by the ultrasonication method [16,34].

Dynamic light scattering analysis showed symmetric and unimodal size distribution curves for all LCNs (see representation in Fig. 1**b**), with PdI values between 0.12 and 0.18. CubLCN and HexLCN showed similar particle sizes of 153.2 (±2.1) and 156.7 (±1.7) nm, respectively. As expected, the presence of PAH resulted in an increase in particle size compared to LCNs without PAH (147.5 ± 2.3 nm and 144.1 ± 1.8 nm for CubLCN and HexLCN, respectively). PAH concentration was determined in a previous study [16], and the colloidal parameters were reproduced in this study for HexLCN. Consistent with our results, the presence of other cationic agents such as polyethyleneimine, poly-ε-lysine, oleylamine, aminolipids, and ionizable lipids also had an influence on the mean particle size of LCNs [14,17,35,36]. The presence of DMA also promoted an increase in particle size of approximately 10 nm in both LCNs, which is consistent with the high rate of drug entrapment. The liquid-crystalline mesostructure of LCNs provides a suitable environment to accommodate hydrophobic molecules such as DMA (log P = 2.8) [15,37–40]. When siRNA was electrostatically adsorbed onto the LCNs, the particle size did not changed, which is due to the compaction of the molecules in the LLC structure of the LCNs.

As for the zeta potential, LCNs commonly have a negative surface charge of approximately −40 mV. This is due to the ionization of the carboxylic terminal group in the MO and OA molecules at pH 7 in the buffer, in addition to the presence of the ethylene oxide units of P407, which lead to absorption of hydroxyl ions from the surrounding aqueous environment [41]. The incorporation of 0.5 % (w/v) PAH into the aqueous phase efficiently promoted a positive surface charge of LCNs, which is necessary for electrostatic complexation with siRNA molecules. Interestingly, in this study, the incorporation of PAH into CubLCN promoted a greater increase in zeta potential (+18.0 ± 1.3 mV) compared to HexLCN (+12.6 ± 1.4 mV). It is suggested that the cubic

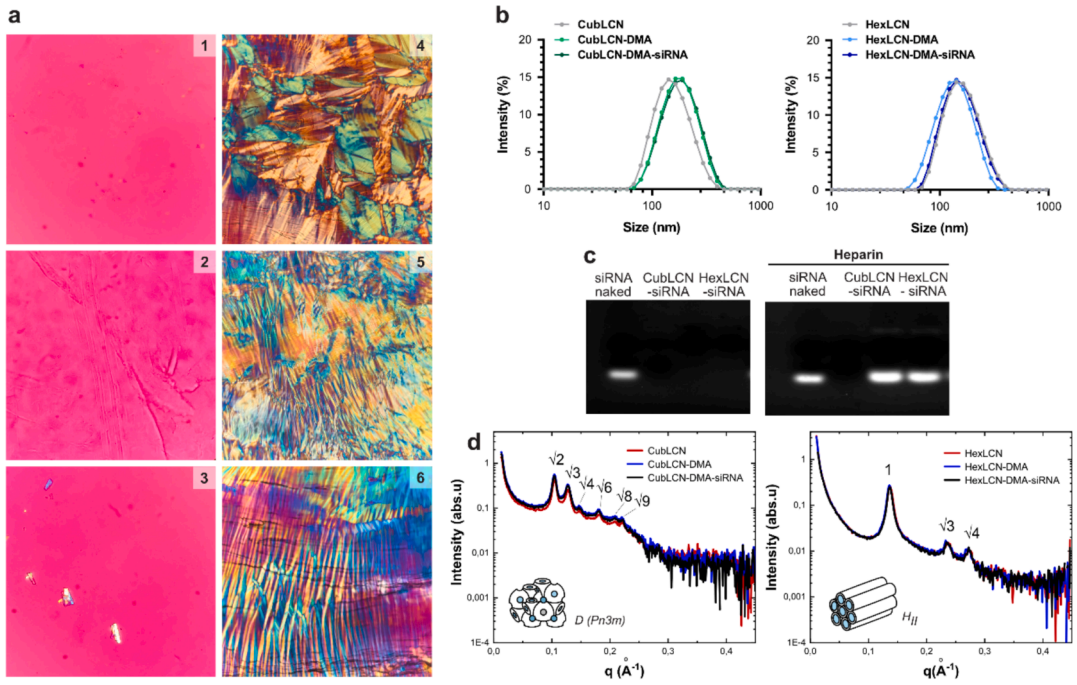

Fig. 1. Characterization of CubLCN and HexLCN. (a) Polarized light microscopy image of the bulk gel: (1) MO:AO:aqueous phase (8:1:90, w/w/w), (2) MO:AO: aqueous phase (8:1:90, w/w/w) with 0.5 % PAH; (3) MO:AO:aqueous phase (8:1:90, w/w) with PAH 0.5 % (w/v) and DMA 0.1 % (w/v). Temperature at 25 °C and objective 32×. **(b)** Representative dynamic light scattering intensity distribution of CubLCN and HexLCN containing or not DMA (0.1 % w/v) and siRNA (10 μM). **(c)** Electrophoretic mobility of siRNA complexed on CubLCN and HexLCN and stability of siRNA released from Cub/HexLCN-siRNA complex following competition with heparin. **(d)** SAXS diffraction patterns of CubLCN and HexLCN containing or not DMA (0.1 % w/v) and siRNA (10 μM). The graphics show the ratio between the interplanar distances and representative illustration of the structural configuration of the bicontinuous cubic (D, diamond) and reverse hexagonal mesophases.

Table 1
Physico-chemical properties of CubLCN and HexLCN.

Formulation	*Z-average (nm)*	*PdI*	*Zeta potential (mV)*	*Concentration (x 10^{12} particles/mL)*	*DMA-EE (%)*	*Lattice parameter (nm)*
CubLCN without PAH	147.5 ± 2.3	0.120 ± 0.006	−40.2 ± 0.6	n.a.	n.a.	n.a.
CubLCN	153.2 ± 2.1	0.120 ± 0.006	+16.8 ± 0.6	7.53 ± 0.43	n.a.	8.53 ± 0.05
CubLCN-DMA	161.3 ± 1.8	0.113 ± 0.004	+18.0 ± 1.3	7.40 ± 0.04	98.10 ± 0.03	8.54 ± 0.05
CubLCN-siRNA	156.1 ± 2.5	0.185 ± 0.007	+15.1 ± 1.2	n.a.	n.a	8.53 ± 0.05
CubLCN-DMA-siRNA	164.8 ± 1.7	0.119 ± 0.003	+15.5 ± 1.1	n.a	n.a.	8.53 ± 0.05
HexLCN without PAH	144.1 ± 1.8	0.113 ± 0.009	−46.6 ± 3.6	n.a.	n.a.	n.a.
HexLCN	156.7 ± 1.7	0.126 ± 0.006	+12.6 ± 1.4	6.12 ± 0.12	n.a.	5.40 ± 0.01
HexLCN-DMA	164.7 ± 1.5	0.179 ± 0.007	+9.9 ± 0.8	6.85 ± 0.15	97.21 ± 0.11	5.35 ± 0.01
HexLCN-siRNA	160.5 ± 1.8	0.161 ± 0.011	+9.1 ± 1.3	n.a.	n.a	5.38 ± 0.01
HexLCN-DMA-siRNA	166.7 ± 1.5	0.179 ± 0.007	+8.9 ± 0.8	n.a	n.a.	5.30 ± 0.01

Abbreviations: DMA = dexamethasone acetate; LCN = liquid-crystalline nanoparticle (Cub for bicontinuous cubic, or Hex for reverse hexagonal mesophase); EE = entrapment efficiency; siRNA = small interfering RNA (1 μM); n.a. = not applicable.
Data are presented by the mean ± standard deviation (n = 3).

mesostructure in combination with the absence of OA (which contains ionized carboxylic terminal groups) favors greater mobility of molecules and ionization of the amine groups of PAH in the diffuse layer of LCNs.

Next, we confirmed the ability of LCNs to complex with siRNA. A slight increase in particle size and PdI was observed, followed by a marginal 2–3 mV decrease in zeta potential. Electrophoretic mobility assays were conducted, and the absence of the characteristic band of naked siRNA indicates a strong association of siRNA with CubLCN or HexLCN, so that it cannot migrate under the influence of the electric field during the gel electrophoresis (Fig. 1**c**). Complexation leads to electroneutralization of the negative charge of the siRNA, which is interesting for the maintenance of high cellular internalization and endosomal escape [42]. The presence of the band was observed after incubation of the LCNs-siRNA complex with heparin, a model polyanion capable of competing with the siRNA, thus mimicking the cellular interior where the siRNA must be de-complexed to be incorporated into the RNAi multiprotein complex. The fluorescence intensity and migration distance similar to naked siRNA indicates that LCN can readily release the siRNA payload without causing its degradation.

As the critical stage of the physicochemical characterization, SAXS measurements were performed to confirm the ordering of the internal mesostructure of the LCNs. Fig. 1**d** shows the 1D scattering patterns and integrated intensities as a function of q for each of the LCNs. SAXS diffraction measurements of CubLCN revealed a diamond-type bicontinuous cubic mesophase (Pn3m), with Bragg peaks indexed at relative positions in the ratios $\sqrt{2}:\sqrt{3}:\sqrt{4}:\sqrt{6}:\sqrt{8}:\sqrt{9}$. For HexLCN, measurements revealed three distinct Bragg peaks with relative positions at $1:\sqrt{3}:\sqrt{4}$ ratio, characteristic of a 2D reverse hexagonal symmetry (p6m).

These SAXS patterns are consistent with what is observed in the literature for LCNs formed only by MO or MO plus OA. At room temperature, hydration of MO in excess of the aqueous phase tends to form bicontinuous cubic mesophases [10,33,43]. A mesophase transition from bicontinuous cubic to hexagonal is achieved with the addition of

fatty acids. In this case, the incorporation of OA is known to reduce lipid layer frustration and leads to a change in the geometry of MO molecules from cylindrical to wedge-shaped, favoring the formation of mesophases with more negative curvature [44–46]. Furthermore, the incorporation of fatty acids such as OA causes flexibility in the structure resulting in smaller particle sizes. Additionally, the SAXS patterns showed that the addition of DMA and siRNA did not affect the internal structure of the bicontinuous cubic or reverse hexagonal LCN mesophases. It is worth mentioning that, unlike other polyanions mentioned in the literature [36,47,48], the presence of the PAH polymer does not cause changes in mean curvature, thus maintaining the LLC mesophase.

The lattice parameter (see Table 1) calculated for CubLCN increased marginally with the presence of DMA, while siRNA complexation maintained values of 8.53 (±0.05) nm. Such results are consistent with those found in the literature with drugs incorporated in the cubic LLC matrix [49–53]. On the other hand, the presence of DMA resulted in a reduction of 0.05 nm in the HexLCN lattice parameter. This dehydration effect suggests that DMA molecules are localized in MO hydrocarbon chains or adsorbed on the surface of inverted micelles, leading to a more negative curvature [16,54,55]. A reduction of approximately 0.02 nm in the lattice parameter of HexLCN or HexLCN-DMA was observed after complexation with siRNA, which is consistent with the attraction of these molecules with PAH in the hydrophilic region of the reverse micelles [16]. These data combined with the polarized light microscopy images, show that the additives in the LLC matrix did not change the magnitude of the spontaneous interfacial curvature of the system, allowing significant structural alterations in the bicontinuous cubic or hexagonal liquid-crystalline mesophase.

3.2. Colloidal and chemical stability of LCNs

After confirming the co-loading of DMA and siRNA in CubLCN and HexLCN, and the maintenance of mesophases in their internal structure after ultrasonication, these LCNs were characterized in terms of stability at room temperature (25 °C) for three months. We evaluated the hydrodynamic diameter, PdI, zeta potential, and encapsulated DMA content, as shown in Fig. 2. The influence of DMA on the stability of LCNs was compared with drug-free LCNs. Overall, the formulations showed good colloidal stability, while there was no significant difference in hydrodynamic diameter and PdI values for at least 30 days, consistent with other studies [16,40,56–59]. CubLCN and CubLCN-DMA showed a significant increase in particle size from day 60 and day 45, respectively, which was accompanied by an increase in PdI. HexLCN and HexLCN-DMA showed slightly better stability, with only a 10–20 nm increase in particle size, indicating that there was no tendency to form aggregates. The fluctuations in PdI values indicate the reorganization of the size distribution of LCNs, although the analyses showed a unimodal distribution with PdI values of 0.165 (±0.006), 0.208 (±0.010), 0.203 (±0.020), and 0.194 (±0.017) for CubLCN, CubLCN-DMA, HexLCN, and HexLCN-DMA respectively.

Zeta potential were measured throughout the stability study period. In particular, the zeta potential ranged from +16.6 (±1.1) to 10.4 (±1.4), +17.3 (±0.8) to 12.3 (±1.7), +10.6 (±1.3) to 7.3 (±0.5), and +10.7 (±1.2) to 8.8 (±1.2) mV for CubLCN, CubLCN-DMA, HexLCN, and HexLCN, respectively. A decrease in zeta potential was observed for CubLCN compared to HexLCN. Overall, these fluctuations in zeta potential did not have a major impact on the colloidal characteristics of the LCNs (little or no aggregation), suggesting that the LCNs have good electrosteric stability. P407 plays a key role in the stability of LCNs due to its organization in the liquid-crystalline structure, where the PEO chains extend outward in the aqueous environment, preventing the aggregation of the particles [12,41].

The encapsulation efficiency was evaluated to obtain a better understanding of the interaction between the DMA and the LCN during long-term storage. As a result of its higher affinity for the hydrophobic region of the LLC matrix, the DMA showed high encapsulation efficiencies (>98 %), which remained constant for at least 45 days. A reduction of 18–25 % in encapsulated content was found from the 45th to the 90th day for CubLCN-DMA, while HexLCN-DMA showed a reduction in DMA content of only 10 %. This behavior may be related to the internal mesostructure of LCN. The structural topology of the inverted hexagonal mesophase consists of seven tightly packed water-filled cylinders, each densely and individually enclosed by a lipid bilayer. This arrangement facilitates the accommodation of DMA and its slow release or leakage. In contrast, the bicontinuous cubic mesophase features long, open, and interconnected water channels in a three-dimensional topology, which may increase the risk of drug leakage [59–62].

3.3. In vitro release kinetics and cutaneous permeation and retention

The release of the incorporated drugs from LCNs depends on the composition, mesophase type, and the intermolecular interactions between components. The topology and diameter of the water channels of the internal mesostructure of LCNs have also been shown to significantly influence the diffusion of the drug [12]. Therefore, the *in vitro* release

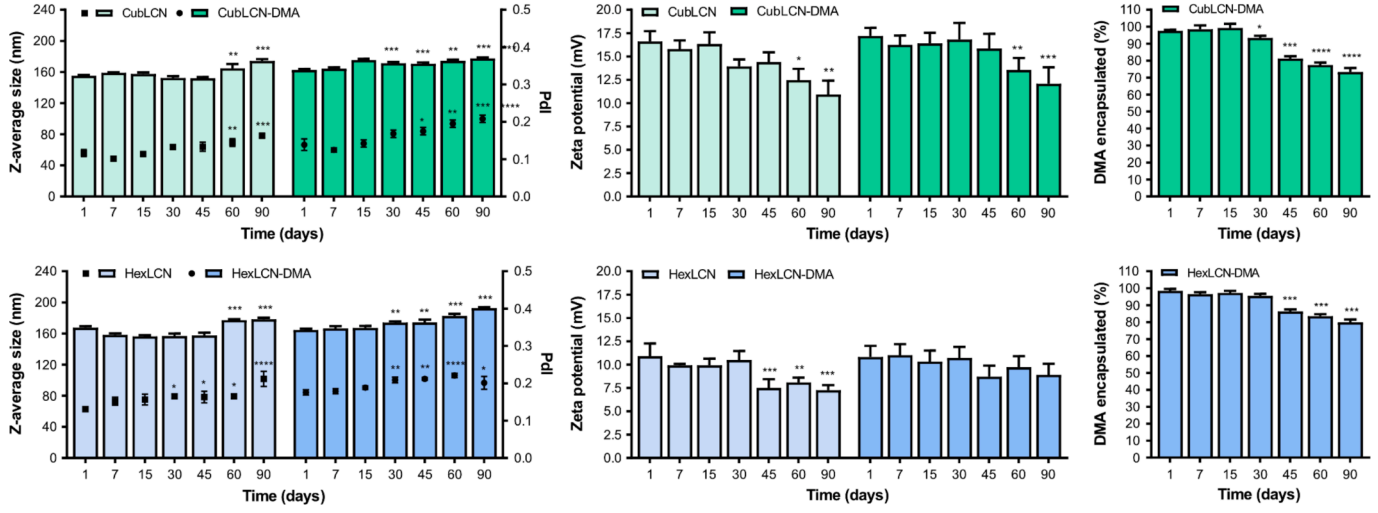

Fig. 2. Physical and chemical stability profile of CubLCN and HexLCN. Z-average size, PdI, zeta potential measurements and encapsulated drug content in CubLCN-DMA and HexLCN-DMA. Data shown are means ± SD (n = 3/3 independent formulations). Statistical analysis was determined by One-way ANOVA, Dunnet's post hoc test (differences compared to 0 day): * $p < 0.01$; ** $p < 0.004$; *** $p < 0.0005$ and **** $p < 0.0001$.

study was performed to determine the effect of the liquid-crystalline mesostructure of LCN on the ability to sustain the release rate of encapsulated DMA. Fig. 3**a** shows the cumulative amount of drug released from the CubLCN and HexLCN as a function of time. DMA was released rapidly from CubLCN, with 73 % of the applied dose being released in 72 h, following zero-order release kinetics ($R^2 = 0.9782$). While DMA in HexLCN was released slowly, totaling 50 % of the dose released in the same period. The release profile was also characterized by zero-order kinetics ($R^2 = 0.9852$); i.e., the same amount of drug is released per unit time, thus promoting a sustained release [63]. A 2.6- to 5.3-fold higher rate was found during the initial 24 h of release for CubLCN-DMA, which indicates that the DMA release rate is affected by the internal mesophase structure of LCN. This behavior is consistent with previous reports describing a faster release of the drug from the bicontinuous cubic mesostructure due to the large surrounding channels, while drugs in the hexagonal mesostructure diffuse more slowly due to the closed water channels with smaller diameters [60–62].

The liquid-crystalline mesostructure can also affect the interaction with biological membranes, such as the skin. In this way, the amount of DMA permeated and retained in dermatomized porcine ear skin was determined and shown in Fig. 3**b**. Approximately 1.4-fold higher amount of DMA was determined in SC (121.6 ± 9.8 μg/cm^2 equivalent to 24 % of the applied initial dose) and an 11.7-fold higher amount of DMA was determined in EPD (40.5 ± 2.7 μg/cm^2 equivalent to 8 % of the applied initial dose) when delivered by HexLCN compared to CubLCN after 24 h of application. Notably, HexLCN promoted a greater drug retention in the skin layers, while the permeated content remained below 1 % of the initial dose, and this was also observed for CubLCN and the free drug solution. Such results are consistent with previous reports and can be explained in part by the high surface area of LCN. Lopes *et al.* obtained a higher cutaneous retention of vitamin K delivered by hexagonal LCN compared to bulk gel [13]. Furthermore, not only the liquid-crystalline mesostructure can influence interactions with membranes, but also the composition of LCNs can promote better drug delivery. The

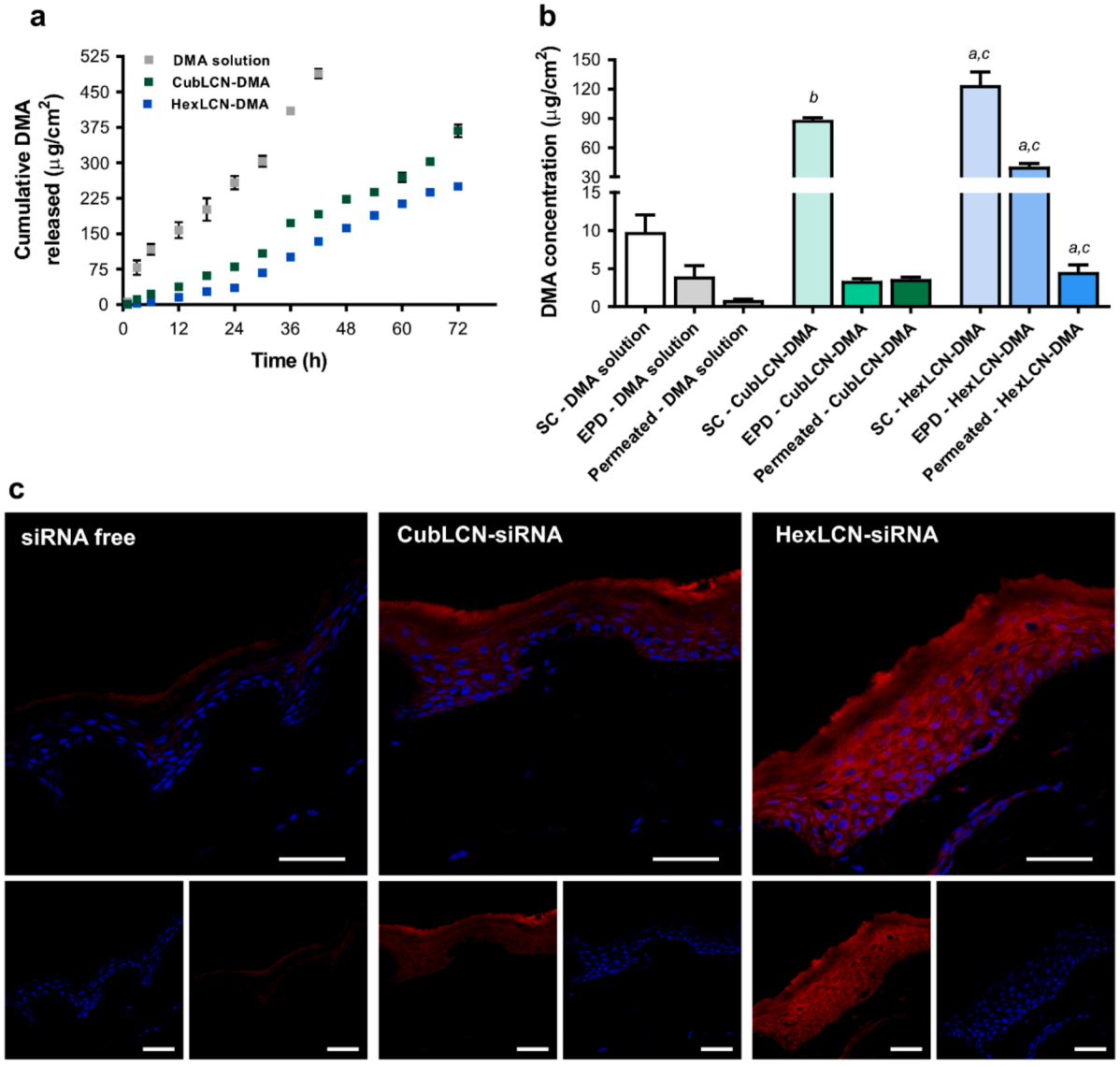

Fig. 3. In vitro topical application of CubLCN-DMA-siRNA and HexLCN-DMA-siRNA using vertical diffusion cell. (a) Cumulative release profile of DMA over time. Data shown are means ± SD (n = 6). **(b)** Concentration of DMA permeated and retained in the stratum corneum (SC) and viable epidermis + dermis (EPD) after 24 h of topical application on dermatomized porcine skin. Statistical analysis was determined by One-way ANOVA, Tukey post hoc test: "*a*" indicates HexLCN-DMA vs solution ($p < 0.0001$); "*b*" indicates CubLCN-DMA vs solution ($p < 0.0001$); and "*c*" indicates HexLCN-DMA vs CubLCN-DMA ($p = 0.0004$). **(c)** Representative CLSM images of porcine skin after 24 h of treatment: siRNA AF647/LCN-siRNA AF647 complex (red – Alexa Fluor 647) and nuclei (blue – DAPI). Scale bar corresponds to 100 μm. (For interpretation of the references to colour in this figure legend, the reader is referred to the web version of this article.)

MO, present in the LCN structure, is known as a penetration enhancer, and its hydrolysis into OA and glycerin results in increased skin hydration, thus expanding penetration through the SC and other layers of the skin [33,43]. Furthermore, it is often suggested that OA disrupts the packing of SC lipids because of its 'kinked' structure resulting from the unsaturated bond. Thus, we believe that the amount of OA added to form the HexLCN structure may have contributed to a significant increase in DMA penetration and retention, due to increased fluidity and reduced diffusional resistance [43,64]. Previously, differences in skin retention of cyclosporine A incorporated into cubic and hexagonal mesophase bulk gels have been reported [88].

Complementing these data, CLSM micrographs of dermatomized skin fragments treated with CubLCN-DMA and HexLCN-DMA complexed with siRNA-labeled AF647 dye demonstrated a predominance of fluorescence throughout the SC and EPD region (Fig. 3**c**). In this assay, the intense red fluorescence in the EPD confirmed that HexLCN has a greater interaction with the skin, allowing for a broader distribution of siRNA AF647 throughout the tissue. Furthermore, we demonstrated that naked siRNA (free solution), being an anionic macromolecule, is unable to penetrate the SC, and its complexation with LCN is essential for reaching the deeper skin layers. Previous reports have confirmed that the skin acts as a barrier to topical siRNA therapy, requiring the use of nanocarriers or physical methods to overcome the SC [8,17,65,66]. To overcome SC, nanoparticles must meet a combination of physicochemical, colloidal, and mechanical factors. In this context, their composition, surface chemistry, and surface charge play a significant role [7,25]. Therefore, in these assays, we demonstrated how CubLCN and HexLCN behave in delivering DMA and siRNA to the skin, with HexLCN showing superior skin penetration of the drugs.

3.4. Cellular studies: Biocompatibility and TNFα downregulation efficiency

The cell viability of Raw264.7 and HaCat cell lines after incubation with LCN and HexLCN loaded or not with DMA was investigated to determine whether the composition and internal mesophase of LCN can influence its biocompatibility. These two cell lines were chosen because macrophages/monocytes of the Raw 264.7 line are commonly used to evaluate formulations for anti-inflammatory therapies, while keratinocytes make up the majority of epidermal skin cells. According to the resazurin assay, which is based on the metabolic activity of cells, a 50 % reduction in cell viability (of both cell lines) was observed at concentrations between 2.1×10^8 and 3.2×10^8 particles/mL for CubLCN and HexLCN, respectively (see Fig. 4**a–d**). Interestingly, the presence of DMA had a positive effect on the viability of cells exposed to HexLCN-DMA (concentrations between 8 and 0.05 μM), shown by the reduced viability at a higher concentration (~6.4×10^8 particle/mL). As previously reported, the presence of DMA in nanoparticles is cytotoxic at high concentrations, exceeding 200 μM [67–69]. However, it is worth considering the intrinsic cytotoxicity of nanoparticles. For example, polymeric nanoparticles affected viability when DMA concentration reached 0.8 μg/mL (equivalent ~2 μM) [70].

In our results, although both colloidal systems are produced with the same components (except for the absence of OA in CubLCNs) and have similar hydrodynamic particle sizes, the different liquid-crystalline structures and surface curvature of the LCNs may influence their interaction with cell membranes, making HexLCNs less toxic than CubLCNs. Tran *et al.* (2015) also observed a similar behavior with LCNs produced with MO and capric acid, suggesting that liquid-crystalline mesophases promote distinct interactions with the membrane, resulting in different degrees of cytotoxicity [71]. The surface architecture of LCNs can influence biological interactions, leading to distinct metabolic effects [72]. Another explanation may also be related to the smaller interfacial area of HexLCN, which determines a small amount of P407 stabilizer distributed on its surface, thus partially affecting the adsorption of proteins and altering the interaction with cells [12,73,74]. For example, the steric coverage of the polymer chain can control lipid mobility, impacting cytotoxicity [75].

In subsequent studies, we evaluated whether HexLCN and CubLCN would present differences in cellular delivery of siRNA. Cells were treated with the same concentrations of both dispersions (2×10^8 particles/mL) complexed with 40 nM AF647 siRNA. As observed in Fig. 4**e, a** higher mean fluorescence intensity of siRNA-AF647 was measured by FACS in cells treated with HexLCN-siRNA for 12 and 24 h compared to cells that received CubLCN-siRNA. Furthermore, reports show that LPS-activated macrophages increase their phagocytic capacity, leading to increased nanomedicine release [68,76,77]. In our results (Fig. 4**f**), the increase in mean siRNA fluorescence at 24 h compared to unstimulated cells clearly demonstrates that endocytic activity contributes to increased uptake, mainly of HexLCN (1.4-fold increase), and this may contribute to increased DMA and siRNA loading in inflammatory environments. Consistent with these data, the CLSM micrographs in Fig. 4**g** clearly show that basal or inflamed cells had greater intensity and distribution of siRNA AF647 throughout the cytoplasm when delivered by HexLCN compared to CubLCN. Therefore, both experimental techniques clearly show that cellular internalization of siRNA-loaded HexLCN was higher and persisted over a longer period of time.

In these results, we again observe how the liquid-crystalline structure of LCNs can be a determining factor in biological interactions, resulting in distinct uptake and cytotoxicity behaviors. According to the literature, the difference in LCN uptake levels may be related to the different entry mechanisms and the different nanoparticle-cell interactions with different structures and morphologies [12,78]. It has been proposed that the elongated shape of HexLCN may favor better adsorption and a greater contact area with the cell membrane compared to other spherical particles [71,79]. A rapid internalization of non-spherical particles, such as HexLCN, is consistent with a recent report by Rodrigues *et al.* (2019) [80]. In addition, it has been proposed that the lipids of the hexagonal mesophase are energetically frustrated (negative curvature), which merges with the lipids of cellular and endosomal membranes [81]. Alternatively, the elasticity of nanoparticles is also a factor that can affect their internalization in different ways, with a greater interaction reported for HexLCN, which have a higher modulus of elasticity than CubLCN (more rigid) [82–85].

For subsequent studies to evaluate the anti-inflammatory potential in an *in vitro* model of inflammation using monocytes/macrophages, we selected HexLCN due to its better cellular delivery capacity of siRNA and cytocompatibility. In this assay, we evaluated the delivery of a specific siRNA targeting TNFα (siTNFα) and tested its combination with DMA to suppress TNFα production. TNFα is a cytokine with pleiotropic effects on various cell types and plays a central role in orchestrating the inflammatory immune response in several diseases [26]. The use of siRNA to silence TNFα has been explored for antipsoriatic therapy [14,22,86], and in skin wound healing [87,88]. Furthermore, as an initial hypothesis, we believe that co-delivery with DMA (glucocorticoid) may lead to a marked reduction in TNFα levels and modulate the inflammatory process. As one of the main stimuli for the production of TNFα is LPS, a molecule in the external membrane of Gram-negative bacteria, we established three different experimental models of induction and treatment of the cells (see schematic illustration in Fig. 5**a**) and quantified the levels of TNFα secreted by these cells after 24 h by ELISA.

In the first protocol, the results presented in Fig. 5b demonstrate that the co-delivery of DMA (1 μM) and siTNFα (150 nM) via HexLCN significantly reduced TNFα secretion compared to the LPS control. Treatment with HexLCN containing each drug alone also showed a decrease in TNFα levels (1066.2 ± 66.8 pg/mL for HexLCN-DMA and 1285.8 ± 45.8 pg/mL for HexLCN-siTNFα), but the combination (HexLCN-DMA-siTNFα) reduced TNFα levels more than 4-fold (635.4 ± 11.8 pg/mL) compared to untreated cells (3082.6 ± 93.2 pg/mL). Similar behavior was observed in cells that received treatments simultaneously with LPS, as shown in Fig. 5**c**. The co-delivery treatment (HexLCN-DMA-siTNFα) achieved the greatest reduction in TNFα levels

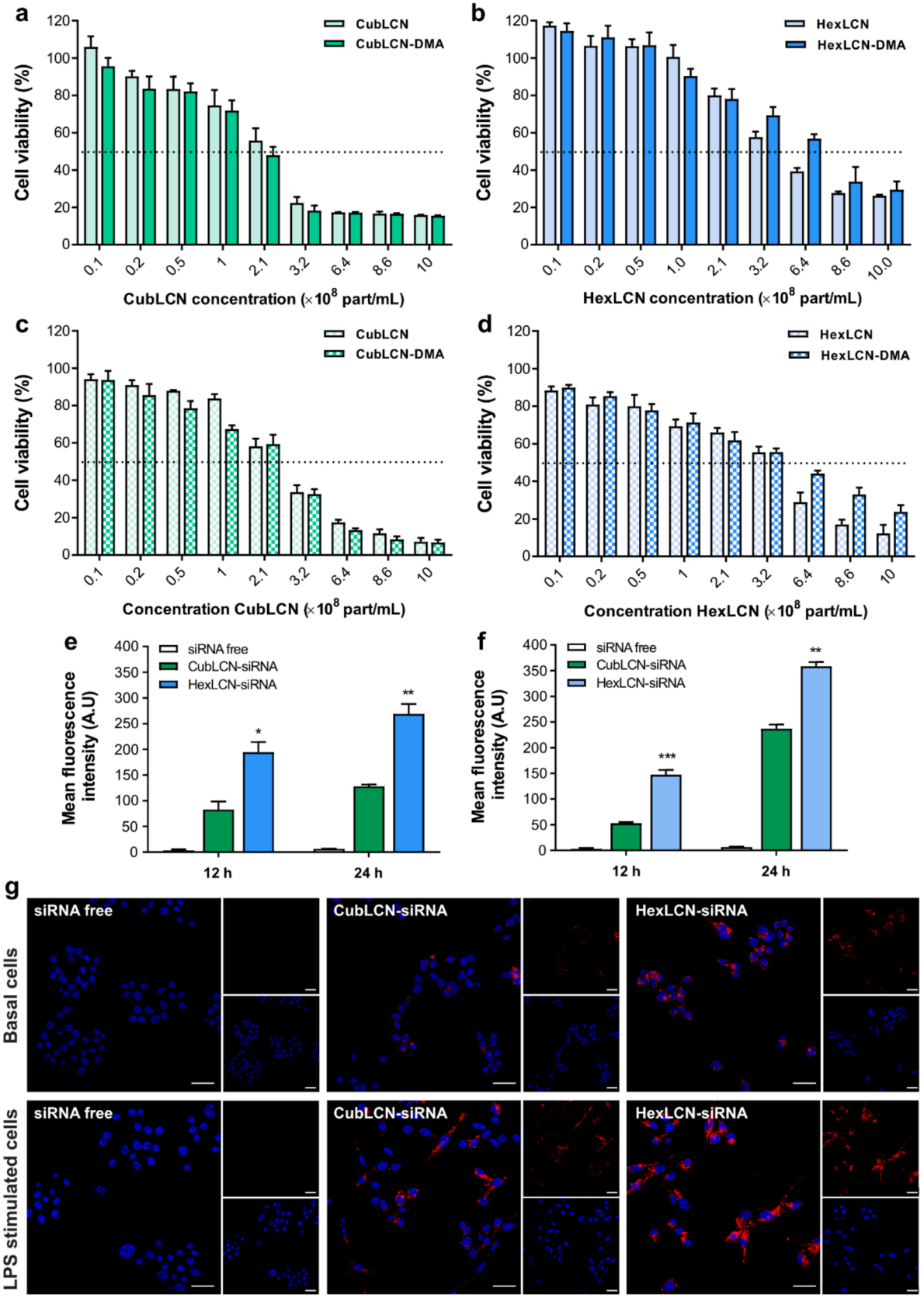

Fig. 4. Cellular studies. Cell viability of **(a-b)** macrophages Raw264.7 cell line and **(c-d)** keratinocytes HaCat cell line after 24 h of treatment with CubLCN, CubLCN-DMA, HexLCN and HexLCN-DMA. Data shown are means ± SD (n = 8). Cell internalization measured by FACS in **(e)** basal cells and **(f)** induced with LPS (5 μg/mL). Data shown are means ± SD (n = 4). Student's *t* test (comparison between HexLCN and CubLCN): * $p < 0.01$; ** $p \leq 0.005$ and *** $p \leq 0.002$. **(g)** Representative CLSM images after 24 h of treatment on basal cells and LPS-stimulated cells. Nuclei (blue – DAPI) and siRNA (red – AlexaFluor 647). Scale bar corresponds to 20 μm. (For interpretation of the references to colour in this figure legend, the reader is referred to the web version of this article.)

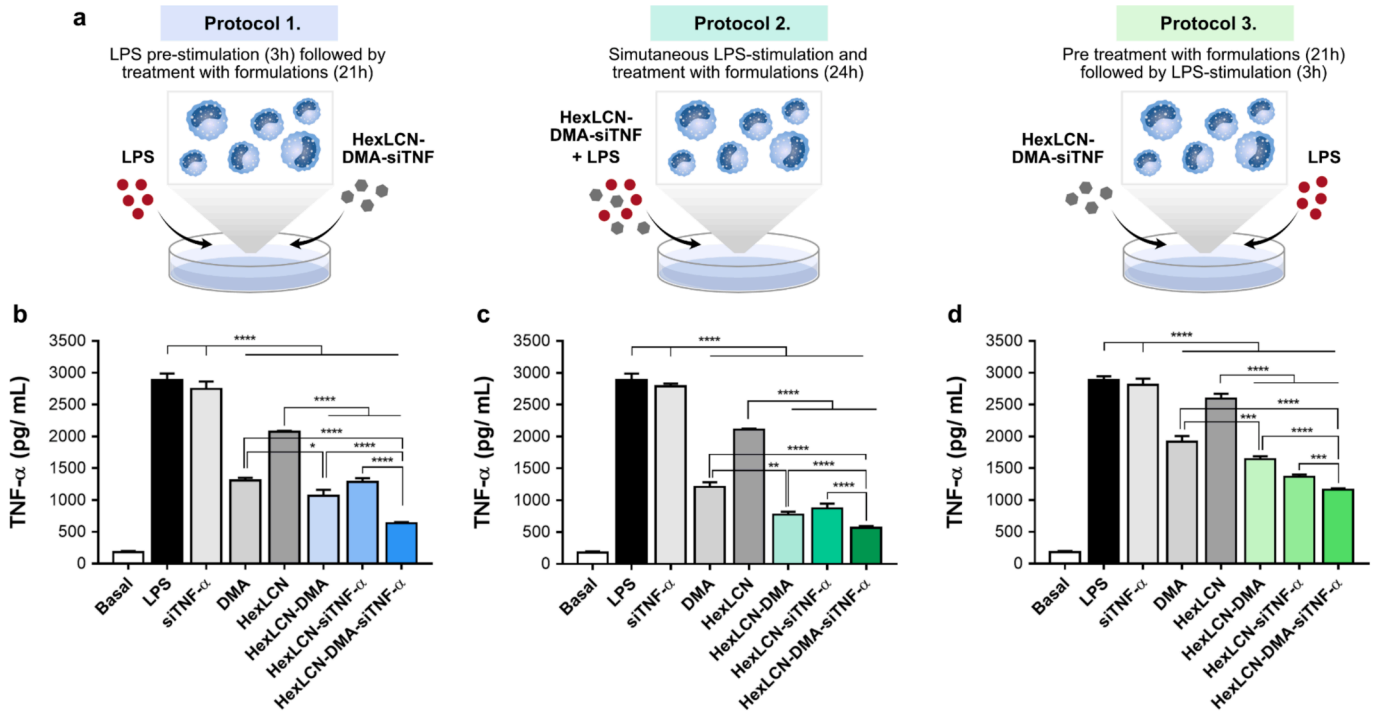

Fig. 5. Effects of HexLCN-DMA-siTNFα on cytokine production in LPS-stimulated Raw264.7 cells. (a) Graphic representation of protocols for evaluating TNFα downregulation efficiency in LPS-stimulated Raw264.7 cells. **(b)** Levels of TNFα secreted in cells pre-stimulated with LPS, followed by treatment with the formulations. **(c)** Levels of TNFα secreted in cells stimulated with LPS and treatment with the formulations simultaneously. **(d)** Levels of TNFα secreted in cells pretreated with the formulations, followed by stimulation with LPS. DMEM culture medium and LPS (500 ng/mL) were used as negative control and positive control, respectively. Data shown are means ± SD (n = 4). One way-ANOVA, Tukey's post test: * $p < 0.05$; ** $p \leq 0.01$; *** $p \leq 0.001$ and **** $p < 0.0001$.

(566.4 ± 20.8 pg/mL), surpassing the effects of monotherapies with HexLCN-siTNFα (870.3 ± 60 pg/mL) and HexLCN-DMA (774.8 ± 30 pg/mL). These findings further highlight the superior efficacy of the dual-drug delivery system in suppressing TNFα secretion.

Furthermore, in the third experimental condition, pre-treatment with HexLCN-DMA-siTNFα before LPS stimulation also proved to be an effective strategy, as shown in Fig. 5**d**. TNFα levels in cells pre-treated with HexLCN-DMA-siTNFα were significantly reduced (1158.5 ± 19.9 pg/mL), representing a 2.5-fold decrease compared to the LPS control (2882.6 ± 52.5 pg/mL). Importantly, this combination therapy outperformed the individual treatments, which resulted in TNFα levels of 1640.3 ± 35 pg/mL (HexLCN-DMA) and 1363.5 ± 25 pg/mL (HexLCN-siTNFα).

In all protocols examined, we showed that siTNFα showed silencing activity only when transported by HexLCN. DMA, well known for its immunomodulatory effects, was able to attenuate TNFα levels, but its delivery by HexLCN showed pronounced effects. Therefore, siTNFα and DMA co-delivered by HexLCN exhibited a synergistic effect in reducing TNFα secretion by macrophages. This effect can be attributed to the mechanisms by which DMA and siTNFα act, i.e. gene transcription and translation. DMA exerts its anti-inflammatory effects by forming a homodimer with GRs, which interact with glucocorticoid response elements in gene promoter regions or interfere with the activity of pro-inflammatory transcription factors such as NF-kappaB (transrepression) [18,19]. Meanwhile, siRNA causes mRNA degradation by binding to the Argonaute protein, forming an RISC that guides the complementary cleavage of specific mRNA sequences, thus preventing protein translation [25].

Due to its potent effects, we selected a low concentration of DMA (1 μM) for our experiments, combined with siTNFα at a concentration known for its knockdown effects [16], which, importantly, did not exhibit immunogenicity. Previous reports have shown that combining glucocorticoids, such as betamethasone or dexamethasone, with siTNFα [89,90], as well as with other nucleic acids [70,91,92], also resulted in superior immunosuppressive effects when co-delivered. However, the dose of DMA used in this study is more than 100-folds lower than those reported in the literature [67,69,90,93], reinforcing the promising efficacy of our combination therapy, which may potentially reduce glucocorticoid-related adverse effects.

Moreover, it is important to highlight that the results found are attributed to the co-delivery by HexLCN and its ability to overcome obstacles such as cellular internalization and endosomal escape. It is well known that one of the major challenges of nucleic acid therapy is the extra- and intracellular barriers, which generally do not exist for other types of bioactive molecules. siRNAs require delivery vehicles that provide protection and deliver therapeutically sufficient amounts to the cytoplasm [25,94]. We attribute to HexLCN abilities rarely found in common nanostructures; for example, the liquid-crystalline mesostructure promotes endosomal escape mechanisms by interacting with lysosomes and endosomes [95,96]. In addition, the presence of PAH induces osmotic swelling of the endosome [16,22,97,98], thus increasing the intracellular bioavailability of drugs. Therefore, HexLCN co-loaded with DMA and siTNFα represents an innovative strategy for the therapy of inflammatory skin diseases involving a complex network of cytokines and other pro-inflammatory mediators.

4. Conclusion

In this study, we successfully prepared DMA-loaded CubLCN and HexLCN by the ultrasonication method and their complexes CubLCN-DMA-siRNA and HexLCN-DMA-siRNA via electrostatic interaction. The dispersions showed small particle size and narrow size distribution, which are suitable for effective topical administration. We showed that reverse hexagonal LCNs have a superior capacity superior ability than cubic LCNs in overcoming the SC and other skin layers, promoting greater penetration of DMA and siRNA. Such abilities were related to their contact surface area, structural similarity with the liquid crystalline structure of the skin, and the presence of oleic acid that favors

partitioning into the SC. Subsequently, *in vitro* cellular studies also confirmed greater cellular internalization of siRNA when complexed with HexLCNs. In addition, in knockdown studies, DMA and siTNFα co-loaded HexLCN promoted an efficient reduction of TNFα levels in LPS-stimulated macrophages under different experimental conditions that mimicked the inflammatory microenvironment.

The results of this study suggest that co-delivery of siTNFα (or any other siRNA targeting pathological skin targets) and DMA may be a potential strategy for the therapy of inflammatory skin diseases involving a complex network of cytokines and pro-inflammatory mediators. Moreover, the multifunctional system is a potential strategy to suppress TNFα, which is one of the key cytokines involved in the initiation and maintenance of inflammation in psoriasis and other inflammatory skin diseases, and the liquid crystalline structure is crucial for the co-delivery of both drugs and nucleic acids. The perspectives of this study focus on solutions to overcome the challenges of large-scale production by more robust methods (e.g. microfluidics), which are of paramount importance for applicability in preclinical investigations. Moreover, studies in psoriatic skin of animal model will bring answers of in vivo behaviors of this therapeutic proposal, including dose and therapeutic protocols."

CRediT authorship contribution statement

Ana Vitória Pupo Silvestrini: Writing – original draft, Validation, Software, Methodology, Investigation, Conceptualization. **Ualisson José da Silva:** Writing – review & editing, Investigation. **Márcia Carvalho de Abreu Fantini:** Writing – review & editing, Software, Methodology. **Maria Vitória Lopes Badra Bentley:** Writing – review & editing, Supervision, Resources, Project administration, Funding acquisition, Conceptualization.

Declaration of competing interest

The authors declare that they have no known competing financial interests or personal relationships that could have appeared to influence the work reported in this paper.

Acknowledgements

This work was developed within the framework of National Institute of Science and Technology of Pharmaceutical Nanotechnology (INCT-Nanofarma), and supported by São Paulo Research Foundation (FAPESP, Brazil, grant #2014/50928-2) and "Conselho Nacional de Desenvolvimento Científico e Tecnológico'' (CNPq, Brazil, grant #465687/2014-8). A.V.P.S. received a FAPESP fellowship (grant #2022/01969-4). The authors thank the Multiuser Facility of the GFCx-Institute of Physics of University of São Paulo for the SAXS measurements.

Data availability

Data will be made available on request.

References

[1] M.G. Netea, F. Balkwill, M. Chonchol, F. Cominelli, M.Y. Donath, E.J. Giamarellos-Bourboulis, D. Golenbock, M.S. Gresnigt, M.T. Heneka, H.M. Hoffman, R. Hotchkiss, L.A.B. Joosten, D.L. Kastner, M. Korte, E. Latz, P. Libby, T. Mandrup-Poulsen, A. Mantovani, K.H.G. Mills, K.L. Nowak, L.A. O'Neill, P. Pickkers, T. van der Poll, P.M. Ridker, J. Schalkwijk, D.A. Schwartz, B. Siegmund, C.J. Steer, H. Tilg, J.W.M. van der Meer, F.L. van de Veerdonk, C.A. Dinarello, A guiding map for inflammation, Nat. Immunol. 18 (2017) 826–831, https://doi.org/10.1038/ni.3790.

[2] V. Prasannanjaneyulu, S. Nene, H. Jain, R. Nooreen, S. Otavi, P. Chitlangya, S. Srivastava, Old drugs, new tricks: Emerging role of drug repurposing in the management of atopic dermatitis, Cytokine Growth Factor Rev. 65 (2022) 12–26, https://doi.org/10.1016/j.cytogfr.2022.04.007.

[3] M. Pasparakis, I. Haase, F.O. Nestle, Mechanisms regulating skin immunity and inflammation, Nat. Rev. Immunol. 14 (2014) 289–301, https://doi.org/10.1038/nri3646.

[4] C. Karimkhani, R.P. Dellavalle, L.E. Coffeng, C. Flohr, R.J. Hay, S.M. Langan, E. O. Nsoesie, A.J. Ferrari, H.E. Erskine, J.I. Silverberg, T. Vos, M. Naghavi, Global skin disease morbidity and mortality, JAMA Dermatol. 153 (2017) 406, https://doi.org/10.1001/jamadermatol.2016.5538.

[5] J.A. Bouwstra, A. Nădăban, W. Bras, C. McCabe, A. Bunge, G.S. Gooris, The skin barrier: An extraordinary interface with an exceptional lipid organization, Prog. Lipid Res. 92 (2023) 101252, https://doi.org/10.1016/j.plipres.2023.101252.

[6] M.S. Roberts, H.S. Cheruvu, S.E. Mangion, A. Alinaghi, H.A.E. Benson, Y. Mohammed, A. Holmes, J. Van Der Hoek, M. Pastore, J.E. Grice, Topical drug delivery : History, percutaneous absorption, and product development, Adv. Drug Deliv. Rev. 177 (2021) 113929, https://doi.org/10.1016/j.addr.2021.113929.

[7] N. Tiwari, E.R. Osorio-Blanco, A. Sonzogni, D. Esporrín-Ubieto, H. Wang, M. Calderón, Nanocarriers for skin applications: where do we stand? Angew. Chemie Int. Ed. 61 (2022) https://doi.org/10.1002/anie.202107960.

[8] A.V.P. Silvestrini, A.L. Caron, J. Viegas, F.G. Praça, M.V.L.B. Bentley, Advances in lyotropic liquid crystal systems for skin drug delivery, Expert Opin. Drug Deliv. 00 (2020) 1–25, https://doi.org/10.1080/17425247.2020.1819979.

[9] V.K. Rapalli, T. Waghule, N. Hans, A. Mahmood, S. Gorantla, S.K. Dubey, G. Singhvi, Insights of lyotropic liquid crystals in topical drug delivery for targeting various skin disorders, J. Mol. Liq. 315 (2020) 113771, https://doi.org/10.1016/j.molliq.2020.113771.

[10] S. Milak, A. Zimmer, Glycerol monooleate liquid crystalline phases used in drug delivery systems, Int. J. Pharm. 478 (2015) 569–587, https://doi.org/10.1016/j.ijpharm.2014.11.072.

[11] A.C. Pham, A.J. Clulow, B.J. Boyd, Formation of self-assembled mesophases during lipid digestion, Front. Cell Dev. Biol. 9 (2021) 1–17, https://doi.org/10.3389/fcell.2021.657886.

[12] A.V.P. Silvestrini, B.W. Debiasi, F.G. Praça, M.V.L.B. Bentley, Progress and challenges of lyotropic liquid crystalline nanoparticles for innovative therapies, Int. J. Pharm. 628 (2022) 122299, https://doi.org/10.1016/j.ijpharm.2022.122299.

[13] R. Mezzenga, J.M. Seddon, C.J. Drummond, B.J. Boyd, G.E. Schröder-Turk, L. Sagalowicz, Nature-inspired design and application of lipidic lyotropic liquid crystals, Adv. Mater. 31 (2019) 1900818, https://doi.org/10.1002/adma.201900818.

[14] R. Petrilli, J.O. Eloy, F.S.G. Praça, J.O. Del Ciampo, M.A.C. Fantini, M.J.V. Fonseca, M.V.L.B. Bentley, Liquid crystalline nanodispersions functionalized with cell-penetrating peptides for topical delivery of short-interfering RNAs: A proposal for silencing a pro-inflammatory cytokine in cutaneous diseases, J. Biomed. Nanotechnol. 12 (2016) 1063–1075, https://doi.org/10.1166/jbn.2016.2211.

[15] P.M. Campos, F.G. Praça, S.V. Mussi, S.A. Figueiredo, M.C. de A. Fantini, M.J. V. Fonseca, V.P. Torchilin, M.V.L.B. Bentley, Liquid crystalline nanodispersion functionalized with cell-penetrating peptides improves skin penetration and anti-inflammatory effect of lipoic acid after in vivo skin exposure to UVB radiation, Drug Deliv. Transl. Res. 10 (2020) 1810–1828, https://doi.org/10.1007/s13346-020-00840-2.

[16] A.V.P. Silvestrini, F. Garcia Praça, M.N. Leite, M.C. de Abreu Fantini, M.A.C. Frade, M.V.L. Badra Bentley, Liquid crystalline nanoparticles enable a multifunctional approach for topical psoriasis therapy by co-delivering triptolide and siRNAs, Int. J. Pharm. 640 (2023) 123019, https://doi.org/10.1016/j.ijpharm.2023.123019.

[17] F.T.M.D.C. Vicentini, L.V. Depieri, A.C.M. Polizello, J.O. Del Ciampo, A.C. C. Spadaro, M.C.A. Fantini, M. Vitória Lopes Badra Bentley, Liquid crystalline phase nanodispersions enable skin delivery of siRNA, Eur. J. Pharm. Biopharm. 83 (2013) 16–24, https://doi.org/10.1016/j.ejpb.2012.08.011.

[18] D.W. Cain, J.A. Cidlowski, Immune regulation by glucocorticoids, Nat. Rev. Immunol. 17 (2017) 233–247, https://doi.org/10.1038/nri.2017.1.

[19] L.M. Franco, M. Gadkari, K.N. Howe, J. Sun, L. Kardava, P. Kumar, S. Kumari, Z. Hu, I.D.C. Fraser, S. Moir, J.S. Tsang, R.N. Germain, Immune regulation by glucocorticoids can be linked to cell type–dependent transcriptional responses, J. Exp. Med. 216 (2019) 384–406, https://doi.org/10.1084/jem.20180595.

[20] M. Oray, K. Abu Samra, N. Ebrahimiadib, H. Meese, C.S. Foster, Long-term side effects of glucocorticoids, Expert Opin. Drug Saf. 15 (2016) 457–465, https://doi.org/10.1517/14740338.2016.1140743.

[21] K. Yamamoto, A. Klossek, R. Flesch, F. Rancan, M. Weigand, I. Bykova, M. Bechtel, S. Ahlberg, A. Vogt, U. Blume-Peytavi, P. Schrade, S. Bachmann, S. Hedtrich, M. Schäfer-Korting, E. Rühl, Influence of the skin barrier on the penetration of topically-applied dexamethasone probed by soft X-ray spectromicroscopy, Eur. J. Pharm. Biopharm. 118 (2017) 30–37, https://doi.org/10.1016/j.ejpb.2016.12.005.

[22] I. Suzuki, M.M. de Araujo, V.S. Bagnato, M.V.L.B. Bentley, TNFα siRNA delivery by nanoparticles and photochemical internalization for psoriasis topical therapy, J. Control. Release (2021), https://doi.org/10.1016/j.jconrel.2021.08.039.

[23] A. Mandal, N. Kumbhojkar, C. Reilly, V. Dharamdasani, A. Ukidve, D.E. Ingber, S. Mitragotri, Treatment of psoriasis with NFKBIZ siRNA using topical ionic liquid formulations, Sci. Adv. 6 (2020) 1–10, https://doi.org/10.1126/sciadv.abb6049.

[24] W.-R. Lee, W.-L. Chou, Z.-C. Lin, C.T. Sung, C.-Y. Lin, J.-Y. Fang, Laser-assisted nanocarrier delivery to achieve cutaneous siRNA targeting for attenuating psoriasiform dermatitis, J. Control. Release 347 (2022) 590–606, https://doi.org/10.1016/j.jconrel.2022.05.032.

[25] A.V.P. Silvestrini, M.F. Morais, B.W. Debiasi, F.G. Praça, M.V.L.B. Bentley, Nanotechnology strategies to address challenges in topical and cellular delivery of siRNAs in skin disease therapy, Adv. Drug Deliv. Rev. 207 (2024) 115198, https://doi.org/10.1016/j.addr.2024.115198.

[26] G. van Loo, M.J.M. Bertrand, Death by TNF: a road to inflammation, Nat. Rev. Immunol. 23 (2023) 289–303, https://doi.org/10.1038/s41577-022-00792-3.
[27] C.E.M. Griffiths, A.W. Armstrong, J.E. Gudjonsson, J.N.W.N. Barker, Psoriasis, Lancet 397 (2021) 1301–1315, https://doi.org/10.1016/S0140-6736(20)32549-6.
[28] G. Meister, T. Tuschl, Mechanisms of gene silencing by double-stranded RNA, Nature 431 (2004) 343–349, https://doi.org/10.1038/nature02873.
[29] D.G. Sashital, J.A. Doudna, Structural insights into RNA interference, Curr. Opin. Struct. Biol. 20 (2010) 90–97, https://doi.org/10.1016/j.sbi.2009.12.001.
[30] Y. Yan, X.-Y. Liu, A. Lu, X.-Y. Wang, L.-X. Jiang, J.-C. Wang, Non-viral vectors for RNA delivery, J. Control. Release (2022) 118159, https://doi.org/10.1016/j.jconrel.2022.01.008.
[31] O. Guidelines, T. No, 428: Skin Absorption: In Vitro Method, OECD (2004), https://doi.org/10.1787/9789264071087-en.
[32] J. Jagielski, Ł. Przysiecka, D. Flak, M. Diak, Z. Pietralik-Molińska, M. Kozak, S. Jurga, G. Nowaczyk, Comprehensive and comparative studies on nanocytotoxicity of glyceryl monooleate- and phytantriol-based lipid liquid crystalline nanoparticles, J. Nanobiotechnol. 19 (2021) 1–18, https://doi.org/10.1186/s12951-021-00913-5.
[33] C.V. Kulkarni, W. Wachter, G. Iglesias-Salto, S. Engelskirchen, S. Ahualli, Monoolein: a magic lipid? PCCP 13 (2011) 3004–3021, https://doi.org/10.1039/C0CP01539C.
[34] G. Bor, S. Salentinig, E. Şahin, B. Nur Ödevci, M. Roursgaard, L. Liccardo, P. Hamerlik, S.M. Moghimi, A. Yaghmur, Cell medium-dependent dynamic modulation of size and structural transformations of binary phospholipid/ω-3 fatty acid liquid crystalline nano-self-assemblies: Implications in interpretation of cell uptake studies, J. Colloid Interface Sci. 606 (2022) 464–479, https://doi.org/10.1016/j.jcis.2021.07.149.
[35] H. Yu, B. Dyett, N. Kirby, X. Cai, M. El Mohamad, S. Bozinovski, C.J. Drummond, J. Zhai, pH-dependent lyotropic liquid crystalline mesophase and ionization behavior of phytantriol-based ionizable lipid nanoparticles, Small 2309200 (2024) 1–10, https://doi.org/10.1002/smll.202309200.
[36] S. Rajesh, J. Zhai, C.J. Drummond, N. Tran, Synthetic ionizable aminolipids induce a pH dependent inverse hexagonal to bicontinuous cubic lyotropic liquid crystalline phase transition in monoolein nanoparticles, J. Colloid Interface Sci. 589 (2021) 85–95, https://doi.org/10.1016/j.jcis.2020.12.060.
[37] H. Badie, H. Abbas, Novel small self-assembled resveratrol-bearing cubosomes and hexosomes: preparation, charachterization, and *ex vivo* permeation, Drug Dev. Ind. Pharm. 44 (2018) 2013–2025, https://doi.org/10.1080/03639045.2018.1508220.
[38] M.M. Gabr, S.M. Mortada, M.A. Sallam, Hexagonal liquid crystalline nanodispersions proven superiority for enhanced oral delivery of rosuvastatin: in vitro characterization and in vivo pharmacokinetic study, J. Pharm. Sci. 106 (2017) 3103–3112, https://doi.org/10.1016/j.xphs.2017.04.060.
[39] S.M. Mohyeldin, M.M. Mehanna, N.A. Elgindy, Superiority of liquid crystalline cubic nanocarriers as hormonal transdermal vehicle: comparative human skin permeation-supported evidence, Expert Opin. Drug Deliv. 13 (2016) 1049–1064, https://doi.org/10.1080/17425247.2016.1182490.
[40] B.K. Yoo, R. Baskaran, T. Madheswaran, P. Sundaramoorthy, H.M. Kim, Entrapment of curcumin into monoolein-based liquid crystalline nanoparticle dispersion for enhancement of stability and anticancer activity, Int. J. Nanomed. 9 (2014) 3119, https://doi.org/10.2147/IJN.S61823.
[41] S.B. Rizwan, D. Assmus, A. Boehnke, T. Hanley, B.J. Boyd, T. Rades, S. Hook, Preparation of phytantriol cubosomes by solvent precursor dilution for the delivery of protein vaccines, Eur. J. Pharm. Biopharm. 79 (2011) 15–22, https://doi.org/10.1016/j.ejpb.2010.12.034.
[42] Y. Sato, H. Matsui, R. Sato, H. Harashima, Neutralization of negative charges of siRNA results in improved safety and efficient gene silencing activity of lipid nanoparticles loaded with high levels of siRNA, J. Control. Release 284 (2018) 179–187, https://doi.org/10.1016/j.jconrel.2018.06.017.
[43] M.T.J. Garcia, D.C.R. Oliveira, J.A. Thomazini, M.V.L.B. Bentley, J.L.C. Lopes, L. B. Lopes, M.C.A. Fantini, J.H. Collett, Liquid crystalline phases of monoolein and water for topical delivery of cyclosporin A: Characterization and study of in vitro and in vivo delivery, Eur. J. Pharm. Biopharm. 63 (2006) 146–155, https://doi.org/10.1016/j.ejpb.2006.02.003.
[44] C. Fong, J. Zhai, C.J. Drummond, N. Tran, Micellar Fd3m cubosomes from monoolein – long chain unsaturated fatty acid mixtures: Stability on temperature and pH response, J. Colloid Interface Sci. 566 (2020) 98–106, https://doi.org/10.1016/j.jcis.2020.01.041.
[45] C. Fong, T. Le, C.J. Drummond, Lyotropic liquid crystal engineering–ordered nanostructured small molecule amphiphileself-assembly materials by design, Chem. Soc. Rev. 41 (2012) 1297–1322, https://doi.org/10.1039/C1CS15148G.
[46] N. Tran, X. Mulet, A.M. Hawley, C. Fong, J. Zhai, T.C. Le, J. Ratcliffe, C. J. Drummond, Manipulating the ordered nanostructure of self-assembled monoolein and phytantriol nanoparticles with unsaturated fatty acids, Langmuir 34 (2018) 2764–2773, https://doi.org/10.1021/acs.langmuir.7b03541.
[47] S. Sarkar, N. Tran, S.K. Soni, C.E. Conn, C.J. Drummond, Size-dependent encapsulation and release of dsDNA from cationic lyotropic liquid crystalline cubic phases, (2020). doi: 10.1021/acsbiomaterials.0c00085.
[48] P. Astolfi, E. Giorgini, F.C. Adamo, F. Vita, S. Logrippo, O. Francescangeli, M. Pisani, Effects of a cationic surfactant incorporation in phytantriol bulk cubic phases and dispersions loaded with the anticancer drug 5-fluorouracil, J. Mol. Liq. 286 (2019) 110954, https://doi.org/10.1016/j.molliq.2019.110954.
[49] M. Mierzwa, A. Cytryniak, P. Krysiński, R. Bilewicz, Lipidic liquid crystalline cubic phases and magnetocubosomes as methotrexate carriers, Nanomaterials 9 (2019), https://doi.org/10.3390/nano9040636.
[50] S. Urandur, V.T. Banala, R.P. Shukla, N. Mittapelly, G. Pandey, N. Kalleti, K. Mitra, S.K. Rath, R. Trivedi, P. Ramarao, P.R. Mishra, Anisamide-anchored lyotropic nano-liquid crystalline particles with AIE effect: A smart optical beacon for tumor imaging and therapy, ACS Appl. Mater. Interfaces 10 (2018) 12960–12974, https://doi.org/10.1021/acsami.7b19109.
[51] P. Astolfi, E. Giorgini, V. Gambini, B. Rossi, L. Vaccari, F. Vita, O. Francescangeli, C. Marchini, M. Pisani, Lyotropic liquid-crystalline nanosystems as drug delivery agents for 5-fluorouracil: structure and cytotoxicity, Langmuir 33 (2017) 12369–12378, https://doi.org/10.1021/acs.langmuir.7b03173.
[52] Y. Fan, H. Chen, Z. Huang, J. Zhu, F. Wan, T. Peng, X. Pan, Y. Huang, C. Wu, Taste-masking and colloidal-stable cubosomes loaded with Cefpodoxime proxetil for pediatric oral delivery, Int. J. Pharm. 575 (2020) 118875, https://doi.org/10.1016/j.ijpharm.2019.118875.
[53] M. Godlewska, A. Majkowska-Pilip, A. Stachurska, J.F. Biernat, D. Gaweł, E. Nazaruk, Voltammetric and biological studies of folate-targeted non-lamellar lipid mesophases, Electrochim. Acta 299 (2019) 1–11, https://doi.org/10.1016/j.electacta.2018.12.164.
[54] I. Amar-Yuli, E. Wachtel, E. Ben Shoshan, D. Danino, A. Aserin, N. Garti, Hexosome and hexagonal phases mediated by hydration and polymeric stabilizer, Langmuir 23 (2007) 3637–3645, https://doi.org/10.1021/la062851b.
[55] L.B. Lopes, D.A. Ferreira, D. De Paula, M.T.J. Garcia, J.A. Thomazini, M.C. A. Fantini, M.V.L.B. Bentley, Reverse hexagonal phase nanodispersion of monoolein and oleic acid for topical delivery of peptides: in vitro and in vivo skin penetration of cyclosporin A, Pharm. Res. 23 (2006) 1332–1342, https://doi.org/10.1007/s11095-006-0143-7.
[56] F.C. Rossetti, M.C.A. Fantini, A.R.H. Carollo, A.C. Tedesco, M.V. Lopes Badra Bentley, Analysis of liquid crystalline nanoparticles by small angle X-Ray diffraction: evaluation of drug and pharmaceutical additives influence on the internal structure, J. Pharm. Sci. 100 (2011) 2849–2857, https://doi.org/10.1002/jps.22522.
[57] M. Chountoulesi, N. Pippa, S. Pispas, E.D. Chrysina, A. Forys, B. Trzebicka, C. Demetzos, Cubic lyotropic liquid crystals as drug delivery carriers: Physicochemical and morphological studies, Int. J. Pharm. 550 (2018) 57–70, https://doi.org/10.1016/j.ijpharm.2018.08.003.
[58] S. Urandur, V.T. Banala, R.P. Shukla, S. Gautam, D. Marwaha, N. Rai, M. Sharma, S. Sharma, P. Ramarao, P.R. Mishra, Theranostic lyotropic liquid crystalline nanostructures for selective breast cancer imaging and therapy, Acta Biomater. 113 (2020) 522–540, https://doi.org/10.1016/j.actbio.2020.06.023.
[59] Q. Luo, T. Lin, C.Y. Zhang, T. Zhu, L. Wang, Z. Ji, B. Jia, T. Ge, D. Peng, W. Chen, A novel glyceryl monoolein-bearing cubosomes for gambogenic acid: Preparation, cytotoxicity and intracellular uptake, Int. J. Pharm. 493 (2015) 30–39, https://doi.org/10.1016/j.ijpharm.2015.07.036.
[60] E. Nazaruk, A. Majkowska-Pilip, M. Godlewska, M. Salamończyk, D. Gawel, Electrochemical and biological characterization of lyotropic liquid crystalline phases – retardation of drug release from hexagonal mesophases, J. Electroanal. Chem. 813 (2018) 208–215, https://doi.org/10.1016/j.jelechem.2018.01.029.
[61] Y. Li, A. Angelova, F. Hu, V.M. Garamus, C. Peng, N. Li, J. Liu, D. Liu, A. Zou, pH Responsiveness of Hexosomes and Cubosomes for Combined Delivery of Brucea javanica Oil and Doxorubicin, Langmuir 35 (2019) 14532–14542, https://doi.org/10.1021/acs.langmuir.9b02257.
[62] S. Phan, W.-K. Fong, N. Kirby, T. Hanley, B.J. Boyd, Evaluating the link between self-assembled mesophase structure and drug release, Int. J. Pharm. 421 (2011) 176–182, https://doi.org/10.1016/j.ijpharm.2011.09.022.
[63] P. Costa, J.M. Sousa Lobo, Modeling and comparison of dissolution profiles, Eur. J. Pharm. Sci. 13 (2001) 123–133, https://doi.org/10.1016/S0928-0987(01)00095-1.
[64] S. Leekumjorn, H.J. Cho, Y. Wu, N.T. Wright, A.K. Sum, C. Chan, The role of fatty acid unsaturation in minimizing biophysical changes on the structure and local effects of bilayer membranes, Biochim. Biophys. Acta - Biomembr. 1788 (2009) 1508–1516, https://doi.org/10.1016/j.bbamem.2009.04.002.
[65] W.R. Lee, S.C. Shen, C.T. Sung, P.Y. Liu, J.Y. Fang, Is the fractional laser still effective in assisting cutaneous macromolecule delivery in barrier-deficient skin? Psoriasis and atopic dermatitis as the disease models, Pharm. Res. 35 (2018), https://doi.org/10.1007/s11095-018-2413-6.
[66] Y.Y. Chun, W.W.R. Tan, M.I.G. Vos, W.K. Chan, H.L. Tey, N.S. Tan, T.T.Y. Tan, Scar prevention through topical delivery of gelatin-tyramine-siSPARC nanoplex loaded in dissolvable hyaluronic acid microneedle patch across skin barrier, Biomater. Sci. 10 (2022) 3963–3971, https://doi.org/10.1039/D2BM00572G.
[67] Y. Xiang, Z. Qiu, Y. Ding, M. Du, N. Gao, H. Cao, H. Zuo, H. Cheng, X. Gao, S. Zheng, W. Wan, X. Huang, K. Hu, Dexamethasone-loaded ROS stimuli-responsive nanogels for topical ocular therapy of corneal neovascularization, J. Control. Release 372 (2024) 874–884, https://doi.org/10.1016/j.jconrel.2024.07.012.
[68] W. Tao, P. Xie, C. Huang, Y. Wang, Y. Huang, Z. Yin, Construction of PLGA nanoparticles modified with RWrNM and DLPC and their application in acute rhinosinusitis, Drug Deliv. Transl. Res. 14 (2024) 1063–1076, https://doi.org/10.1007/s13346-023-01450-4.
[69] M. Ji, H. Liu, M. Wei, D. Shi, J. Gou, T. Yin, H. He, X. Tang, C. Chen, Y. Zhang, Redox-sensitive disulfide-bridged self-assembled nanoparticles of dexamethasone with high drug loading for acute lung injury therapy, Int. J. Pharm. 664 (2024) 124600, https://doi.org/10.1016/j.ijpharm.2024.124600.
[70] T. Wan, Q. Pan, Y. Ping, Microneedle-assisted genome editing: A transdermal strategy of targeting NLRP3 by CRISPR-Cas9 for synergistic therapy of inflammatory skin disorders, Sci. Adv. 7 (2021), https://doi.org/10.1126/sciadv.abe2888.
[71] N. Tran, X. Mulet, A.M. Hawley, T.M. Hinton, S.T. Mudie, B.W. Muir, E. C. Giakoumatos, L.J. Waddington, N.M. Kirby, C.J. Drummond, Nanostructure and cytotoxicity of self-assembled monoolein–capric acid lyotropic liquid crystalline

nanoparticles, RSC Adv. 5 (2015) 26785–26795, https://doi.org/10.1039/C5RA02604K.
[72] S. Deshpande, N. Singh, Influence of cubosome surface architecture on its cellular uptake mechanism, Langmuir 33 (2017) 3509–3516, https://doi.org/10.1021/acs.langmuir.6b04423.
[73] S. Murgia, A.M. Falchi, M. Mano, S. Lampis, R. Angius, A.M. Carnerup, J. Schmidt, G. Diaz, M. Giacca, Y. Talmon, M. Monduzzi, Nanoparticles from lipid-based liquid crystals: Emulsifier influence on morphology and cytotoxicity, J. Phys. Chem. B 114 (2010) 3518–3525, https://doi.org/10.1021/jp9098655.
[74] J. Barauskas, C. Cervin, M. Jankunec, M. Špandyreva, K. Ribokaitė, F. Tiberg, M. Johnsson, Interactions of lipid-based liquid crystalline nanoparticles with model and cell membranes, Int. J. Pharm. 391 (2010) 284–291, https://doi.org/10.1016/j.ijpharm.2010.03.016.
[75] A. Tan, L. Hong, J.D. Du, B.J. Boyd, Self-assembled nanostructured lipid systems: is there a link between structure and cytotoxicity? Adv. Sci. 6 (2019) 1801223 https://doi.org/10.1002/advs.201801223.
[76] P. Song, C. Yang, J.S. Thomsen, F. Dagnæs-Hansen, M. Jakobsen, A. Brüel, B. Deleuran, J. Kjems, Lipidoid-siRNA nanoparticle-mediated IL-1β gene silencing for systemic arthritis therapy in a mouse model, Mol. Ther. 27 (2019) 1424–1435, https://doi.org/10.1016/j.ymthe.2019.05.002.
[77] R. Xu, C. Xia, X. He, C. Hu, Y. Li, Y. Zhang, Z. Chen, siRNA nanoparticle dry powder formulation with high transfection efficiency and pulmonary deposition for acute lung injury treatment, ACS Appl. Mater. Interfaces 16 (2024) 54344–54358, https://doi.org/10.1021/acsami.4c04241.
[78] S.L. Yap, H. Yu, S. Li, C.J. Drummond, C.E. Conn, N. Tran, Cell interactions with lipid nanoparticles possessing different internal nanostructures: Liposomes, bicontinuous cubosomes, hexosomes, and discontinuous micellar cubosomes, J. Colloid Interface Sci. 656 (2024) 409–423, https://doi.org/10.1016/j.jcis.2023.11.059.
[79] B.J. Boyd, S.B. Rizwan, Y. Da Dong, S. Hook, T. Rades, Self-assembled geometric liquid-crystalline nanoparticles imaged in three dimensions: Hexosomes are not necessarily flat hexagonal prisms, Langmuir 23 (2007) 12461–12464, https://doi.org/10.1021/la7029714.
[80] L. Rodrigues, F. Schneider, X. Zhang, E. Larsson, L.W.K. Moodie, H. Dietz, C. M. Papadakis, G. Winter, R. Lundmark, M. Hubert, Cellular uptake of self-assembled phytantriol-based hexosomes is independent of major endocytic machineries, J. Colloid Interface Sci. 553 (2019) 820–833, https://doi.org/10.1016/j.jcis.2019.06.045.
[81] K. Ewert, A. Ahmad, H.M. Evans, C.R. Safinya, Cationic lipid–DNA complexes for non-viral gene therapy: relating supramolecular structures to cellular pathways, Expert Opin. Biol. Ther. 5 (2005) 33–53, https://doi.org/10.1517/14712598.5.1.33.
[82] X. Banquy, F. Suarez, A. Argaw, J. Rabanel, P. Grutter, J.-F. Bouchard, P. Hildgen, S. Giasson, Effect of mechanical properties of hydrogel nanoparticles on macrophage cell uptake, Soft Matter 5 (2009) 3984, https://doi.org/10.1039/b821583a.
[83] P. Pitzalis, M. Monduzzi, N. Krog, H. Larsson, H. Ljusberg-Wahren, T. Nylander, Characterization of the liquid−crystalline phases in the glycerol monooleate/diglycerol monooleate/water system, Langmuir 16 (2000) 6358–6365, https://doi.org/10.1021/la0002031.
[84] Y. Hui, X. Yi, D. Wibowo, G. Yang, A.P.J. Middelberg, H. Gao, C.-X. Zhao, Nanoparticle elasticity regulates phagocytosis and cancer cell uptake, Sci. Adv. 6 (2020) 1–11, https://doi.org/10.1126/sciadv.aaz4316.
[85] Z. Shen, H. Ye, X. Yi, Y. Li, Membrane wrapping efficiency of elastic nanoparticles during endocytosis: size and shape matter, ACS Nano 13 (2019) 215–228, https://doi.org/10.1021/acsnano.8b05340.
[86] J.S.R. Viegas, F.G. Praça, A.L. Caron, I. Suzuki, A.V.P. Silvestrini, W.S.G. Medina, J. O. Del Ciampo, M. Kravicz, M.V.L.B. Bentley, Nanostructured lipid carrier co-delivering tacrolimus and TNF-α siRNA as an innovate approach to psoriasis, Drug Deliv. Transl. Res. (2020), https://doi.org/10.1007/s13346-020-00723-6.
[87] Q. Liu, Y. Zhang, J. Huang, Z. Xu, X. Li, J. Yang, H. Huang, S. Tang, Y. Chai, J. Lin, C. Yang, J. Liu, S. Lin, Mesoporous silica-coated silver nanoparticles as ciprofloxacin/siRNA carriers for accelerated infected wound healing, J. Nanobiotechnol. 20 (2022) 386, https://doi.org/10.1186/s12951-022-01600-9.
[88] L.N. Kasiewicz, K.A. Whitehead, Silencing TNFα with lipidoid nanoparticles downregulates both TNFα and MCP-1 in an in vitro co-culture model of diabetic foot ulcers, Acta Biomater. 32 (2016) 120–128, https://doi.org/10.1016/j.actbio.2015.12.023.
[89] H.L. O'Mary, M.S. Hanafy, A.M. Aldayel, S.A. Valdes, R.F. Alzhrani, S. Hufnagel, J. J. Koleng, Z. Cui, Effect of the ratio of betamethasone to TNF-α siRNA coencapsulated in solid lipid nanoparticles on the acute proinflammatory activity of the nanoparticles, Mol. Pharm. 16 (2019) 4496–4506, https://doi.org/10.1021/acs.molpharmaceut.9b00629.
[90] S. Gürcan, N. Tsapis, F. Reynaud, S. Denis, J. Vergnaud, Ö. Özer, E. Fattal, Combining dexamethasone and TNF-α siRNA within the same nanoparticles to enhance anti-inflammatory effect, Int. J. Pharm. 598 (2021) 120381, https://doi.org/10.1016/j.ijpharm.2021.120381.
[91] Q. Wang, H. Jiang, Y. Li, W. Chen, H. Li, K. Peng, Z. Zhang, X. Sun, Targeting NF-kB signaling with polymeric hybrid micelles that co-deliver siRNA and dexamethasone for arthritis therapy, Biomaterials 122 (2017) 10–22, https://doi.org/10.1016/j.biomaterials.2017.01.008.
[92] M. Hou, X. Wu, Z. Zhao, Q. Deng, Y. Chen, L. Yin, Endothelial cell-targeting, ROS-ultrasensitive drug/siRNA co-delivery nanocomplexes mitigate early-stage neutrophil recruitment for the anti-inflammatory treatment of myocardial ischemia reperfusion injury, Acta Biomater. 143 (2022) 344–355, https://doi.org/10.1016/j.actbio.2022.02.018.
[93] C. Li, J. Li, Y. Bai, K. Zhang, Z. Wang, Y. Zhang, Q. Guan, S. Wang, Z. Li, Z. Li, L. Chen, Polysialic acid-based nanoparticles for enhanced targeting and controlled dexamethasone release in pulmonary inflammation treatment, Int. J. Biol. Macromol. 297 (2025) 139550, https://doi.org/10.1016/j.ijbiomac.2025.139550.
[94] S.F. Dowdy, Overcoming cellular barriers for RNA therapeutics, Nat. Biotechnol. 35 (2017) 222–229, https://doi.org/10.1038/nbt.3802.
[95] C. Leal, N.F. Bouxsein, K.K. Ewert, C.R. Safinya, Highly efficient gene silencing activity of siRNA embedded in a nanostructured gyroid cubic lipid matrix, J. Am. Chem. Soc. 132 (2010) 16841–16847, https://doi.org/10.1021/ja1059763.
[96] H. Kim, C. Leal, Cuboplexes: topologically active siRNA delivery, ACS Nano 9 (2015) 10214–10226, https://doi.org/10.1021/acsnano.5b03902.
[97] P. Andreozzi, E. Diamanti, K.R. Py-Daniel, P.R. Cáceres-Vélez, C. Martinelli, N. Politakos, A. Escobar, M. Muzi-Falconi, R. Azevedo, S.E. Moya, Exploring the pH Sensitivity of Poly(allylamine) Phosphate Supramolecular Nanocarriers for Intracellular siRNA Delivery, ACS Appl. Mater. Interfaces 9 (2017) 38242–38254, https://doi.org/10.1021/acsami.7b11132.
[98] D. Di Silvio, M. Martínez-Moro, C. Salvador, M. de los Angeles Ramirez, P. R. Caceres-Velez, M.G. Ortore, D. Dupin, P. Andreozzi, S.E. Moya, Self-assembly of poly(allylamine)/siRNA nanoparticles, their intracellular fate and siRNA delivery, J. Colloid Interface Sci. 557 (2019) 757–766, https://doi.org/10.1016/j.jcis.2019.09.082.